Systematics of even-even $T_z = 1$ nuclei in the $A = 80$ region: High-spin rotational bands in ^{74}Kr, ^{78}Sr, and ^{82}Zr

D. Rudolph,[1,2] C. Baktash,[1] C. J. Gross,[1,3] W. Satula,[4,5,6] R. Wyss,[7] I. Birriel,[8] M. Devlin,[9] H.-Q. Jin,[1,*] D. R. LaFosse,[9] F. Lerma,[9] J. X. Saladin,[8] D. G. Sarantites,[9] G. N. Sylvan,[10] S. L. Tabor,[10] D. F. Winchell,[8] V. Q. Wood,[8] and C. H. Yu[1]

[1]*Physics Division, Oak Ridge National Laboratory, Oak Ridge, Tennessee 37831*
[2]*Sektion Physik der Ludwig-Maximilians-Universität München, D-85748 Garching, Germany*
[3]*Oak Ridge Institute for Science and Education, Oak Ridge, Tennessee 37831*
[4]*Department of Physics, University of Tennessee, Knoxville, Tennessee 37996*
[5]*Joint Institute for Heavy Ion Research, Oak Ridge National Laboratory, Oak Ridge, Tennessee 37831*
[6]*Institute of Theoretical Physics, Warsaw University, PL-00681 Warsaw, Poland*
[7]*The Royal Institute of Technology, Physics Department Frescati, S-104 05 Stockholm, Sweden*
[8]*Department of Physics and Astronomy, University of Pittsburgh, Pittsburgh, Pennsylvania 15260*
[9]*Chemistry Department, Washington University, St. Louis, Missouri 63130*
[10]*Department of Physics, Florida State University, Tallahassee, Florida 32306*

(Received 19 February 1997)

High-spin states of $T_z = 1$ nuclei were studied with the reactions ^{58}Ni(^{28}Si,3α)^{74}Kr, ^{58}Ni(^{28}Si,2α)^{78}Sr, and ^{58}Ni(^{28}Si,2p2n)^{82}Zr at 130 MeV beam energy. The Gammasphere array in conjunction with the 4π charged-particle detector array Microball was used to detect γ rays in coincidence with evaporated light charged particles. The known $\pi = +$, $\alpha = 0$ yrast bands were extended to $I = 28\hbar$ at 20 MeV excitation energy. For all three nuclei, a number of positive- and negative-parity sidebands were established; altogether 15 new rotational bands were found. The data are discussed using the pairing-and-deformation self-consistent total Routhian surface (TRS) model: High-spin structures of ^{74}Kr and ^{78}Sr are governed by the shell gaps at large prolate deformation while ^{82}Zr seems to exhibit shape coexistence. Nearly identical bands were established which may be explained as arising from the fp orbits acting as spectators at very elongated shapes. The experimental data in these $T_z = 1$ nuclei are in good agreement with predictions of the TRS model using conventional $T = 1$ like-nucleon pairing correlations. [S0556-2813(97)01407-6]

PACS number(s): 21.10.Re, 21.60.−n, 23.20.Lv, 27.50.+e

I. INTRODUCTION

The mass region $A \approx 80$ is known to provide a variety of nuclear structure phenomena. Due to the low density of single-particle energy levels, the nuclear shapes are strongly configuration dependent. They are predicted to vary not only with the particle number, but also with excitation energy and spin. According to the mean-field models the structure of the $A \approx 80$ nuclei is governed by large shell gaps of $\approx$ 2 MeV at oblate ($\beta_2 \approx -0.3$, particle numbers 34, 36) and prolate ($\beta_2 \approx +0.4$, particle numbers 38, 40) shapes [1–3]. These shell gaps lead to a large negative shell correction which counterbalances the increase in the smooth component of the nuclear energy due to deformation. Consequently, the ground states of certain Kr, Rb, and Sr isotopes are predicted to be very elongated [1–3]. For some nuclei theory predicts prolate-oblate shape coexistence as well as strong shape-mixing phenomena (see [4,5]). Many theoretical predictions have already been confirmed experimentally. Strong candidates for oblate rotational bands were reported for the $N = Z = 36$ nucleus ^{72}Kr [6,7] and in the light Se ($Z = 34$) isotopes [8]. Another indication for oblate deformation in this mass region is the measured g factor at the first crossing in the positive-parity yrast cascade in ^{78}Kr [9]. The small precession indicates that the aligning nucleons are neutrons which suggests that ^{78}Kr has a near-oblate shape throughout the ground-state band. Large prolate deformations were identified via γ-ray spectroscopy in light Sr nuclei [10], and by means of collinear laser spectroscopy in the Rb ($Z = 37$) [11] and Sr ($Z = 38$) [12,13] isotopic chains. Large transition strengths deduced from lifetime measurements of excited states in a number of rotational bands in the region $Z = 35$–38, $N = 38$–42 (e.g., [14–16]) provide further evidence for the presence of large collectivity in these nuclei. Shape coexisting prolate or oblate shapes as well as single-particle structures have been observed separately in the same nucleus (e.g., ^{82}Sr [17–19]) or were found to mix within the ground-state band (e.g., ^{74}Kr [7,20,21] or ^{86}Zr [22]). In addition to the predicted and observed large normally deformed shell gaps, a long predicted [1,2] island of superdeformed prolate spheroids ($\beta_2 \approx 0.55$) centered around neutron numbers $N \approx 44$ in the Sr to Zr isotopes was recently observed [23–25].

Large shell gaps imply reduced pairing correlations and this is one subject to be addressed in this study for even-even nuclei. Reduced pairing is believed to be responsible for the near-rigid rotation observed in the positive-parity yrast band in ^{77}Rb [16,26] and the negative-parity yrast bands in ^{76}Kr

*Present address: NASA Ames Research Center, Moffett Field, CA 94035.

TABLE I. Off-line sorted E_γ-E_γ matrices (M) and E_γ-E_γ-E_γ cubes (C) used in the analysis.

	Ge-detector angles			Range	Target		Gating		Number of	
	Θ_1 (°)	Θ_2 (°)	Θ_3 (°)	E_γ (keV)	Thin	Thick	p	α	events	Purpose
C	All	All	All	100–2000	×		2	0	2.9×10^8	Level scheme
C	All	All	All	100–2800	×		2	0	3.6×10^8	Level scheme
M	All	All		50–2500	×		2	0	1.2×10^9	Level scheme
M	All	All	[a]	50-2500	×		2	0	1.4×10^6	Level scheme
M	All	All		50–2500		×	2	0	3.0×10^8	Level scheme
M	All	All	[b]	50-2500		×	2	0	1.3×10^6	Level scheme
M	F/B [c]	MI [d]		50–2500	×		2	0	2.9×10^8	DCO ratios
M	F/B [c]	MI [d]		50–2500		×	2	0	6.1×10^7	DCO ratios
M	31.7, 37.4	All		50–2500		×	2	0	1.1×10^8	DSA lifetimes
M	142.6, 148.3	All		50–2500		×	2	0	9.8×10^7	DSA lifetimes
C	All	All	All	100-2800	×		0	2	1.9×10^7	Level scheme
M	All	All		50–2500	×		0	2	3.9×10^7	Level scheme
M	All	All	[e]	50–2500	×		0	2	1.5×10^6	Level scheme
M	All	All		50–2500		×	0	2	6.5×10^6	Level scheme
M	F/B [c]	MI [d]		50–2500	×		0	2	7.9×10^6	DCO ratios
M	F/B [c]	MI [d]		50–2500		×	0	2	1.3×10^6	DCO ratios
C	All	All	All	100–2800	×		0	2-3	2.1×10^7	Level scheme
M	All	All		50–2500	×		0	3	3.5×10^6	Level scheme
M	All	All		50–3300	×		0	3	3.7×10^6	Level scheme
M	F/B [c]	MI [d]		50–2500	×		0	2-3	8.6×10^6	DCO ratios
M	F/B [c]	MI [d]		50–2500		×	0	2-3	1.4×10^6	DCO ratios

[a]Gated with a third γ ray at 407 or 634 keV.
[b]Gated with a third γ ray at 407, 634, 847, or 1021 keV.
[c]31.7, 37.4, 50.1, 129.9, 142.6, 148.3, and 162.7.
[d]79.2, 80.7, 90.0, 99.3, and 100.8.
[e]Gated with a third γ ray at 278, 503, 712, or 895 keV.

[15]. The effects of the shell gaps should be reinforced in the self-conjugate $N=Z$ nuclei. In addition, the $T=0$ neutron-proton (n-p) pairing mode in the even-even $N=Z$ nuclei is suggested to influence the expected band-crossing pattern [27]. Alongside this collective $T=0$ pairing correlation (a clear signature of which is yet to be determined) stands the possibility of a strong residual (noncollective) $T=0$ interaction between valence protons and neutrons moving in identical orbitals. Recently, a signature of $T=1$ and $T=0$ band crossings was likewise observed in the odd-odd $N=Z$ nucleus ^{74}Rb [28]. Unfortunately, the cross sections for populating $N=Z$ nuclei in the $A=80$ region with stable beam-target combinations are on the order of 10–100 μb and the fusion-evaporation reactions at energies near the Coulomb barrier used in the past [29,30] do not provide enough angular momentum to observe the complete alignment into the 4 quasiparticle (qp) region. As compared to the $N=Z$ nuclei the $T_z=1$ nuclei have much larger cross sections (about 1 mb) which allow extensive studies up to high angular momenta by using the γ-detector arrays of the latest generation. Though the collective n-p pairing is predicted to decrease rapidly when moving away from the $N=Z$ line [31–33], the $T_z=1$ nuclei may still contain a sizable amount of that strength. There are also possible configurations, espe-

TABLE II. Experimental relative cross sections for the reaction ^{28}Si+^{58}Ni at $\overline{E_{\rm beam}}=128$ MeV deduced from the yields of known ground-state and bandhead transitions in various particle-gated spectra.

Reaction channel	$\sigma_{\rm rel}$ (%)	Reaction channel	$\sigma_{\rm rel}$ (%)	Reaction channel	$\sigma_{\rm rel}$ (%)	Reaction channel	$\sigma_{\rm rel}$ (%)	Reaction channel	$\sigma_{\rm rel}$ (%)
^{73}Br+3αp	0.080(8)	^{78}Kr+α4p	1.1(1)	^{80}Rb+5pn	0.033(8)	^{80}Sr+α2p	14(1)	^{82}Y+3pn	5.3(3)
^{75}Br+2α3p	0.047(11)	^{80}Kr+6p	$<$0.006	^{81}Rb+5p	0.77(12)	^{81}Sr+4pn	4.9(3)	^{83}Y+3p	6.7(10)
^{74}Kr+3α	0.21(1)	^{76}Rb+2αpn	0.094(9)	^{76}Sr+2α2n	$<$0.002	^{82}Sr+4p	13(1)	^{80}Zr+α2n	$<$0.003
^{75}Kr+2α2pn	0.014(4)	^{77}Rb+2αp	6.1(4)	^{77}Sr+2αn	0.022(3)	^{79}Y+αp2n	$<$0.05	^{82}Zr+2p2n	0.40(7)
^{76}Kr+2α2p	5.7(4)	^{78}Rb+α3pn	0.80(11)	^{78}Sr+2α	0.14(5)	^{80}Y+αpn	0.28(6)	^{83}Zr+2pn	0.58(4)
^{77}Kr+α4pn	0.045(5)	^{79}Rb+α3p	33(2)	^{79}Sr+α2pn	4.6(5)	^{81}Y+3p2n	1.2(1)	^{84}Zr+2p	0.10(1)

TABLE III. The energies of excited states in ^{74}Kr, the transitions energies and relative intensities of the γ rays placed in the level scheme, the DCO ratios and the gate used to obtain them, and the spins and parities of the initial and final states of the γ rays.

E_x (keV)	E_γ (keV)	$I_{\rm rel}$ (%)	$R_{\rm DCO}$	Gate [a]	I_i^π ($\hbar$)	I_f^π ($\hbar$)	E_x (keV)	E_γ (keV)	$I_{\rm rel}$ (%)	$R_{\rm DCO}$	Gate [a]	I_i^π ($\hbar$)	I_f^π ($\hbar$)
455.6(1)	455.6(1)	100(3)			2^+	0^+		1585.7(3)	10(1)	0.56(5)	*B,F*	7^-	6^+
1013.3(1)	557.7(1)	89(3)	0.95(2)	*A,D*	4^+	2^+	4132.8(4)	766.9(5)	17(3)	[b]		9^-	7^-
1781.4(2)	768.0(2)	72(5)	1.07(2)	*B,D*	6^+	4^+		1384.3(4)	4.2(4)	0.57(10)	*B,E*	9^-	8^+
2747.9(2)	966.5(1)	56(2)	1.05(3)	*B,D*	8^+	6^+	5086.3(4)	953.5(2)	17(1)	1.01(5)	*B,F*	11^-	9^-
3892.3(3)	1144.4(1)	44(2)	1.01(3)	*B,D*	10^+	8^+	6210.5(5)	1124.2(2)	16(1)	0.96(6)	*B,F*	13^-	11^-
5179.5(3)	1287.2(2)	35(2)	1.07(4)	*B,D*	12^+	10^+	7487.5(6)	1277.0(3)	14(1)	1.08(6)	*E,F*	15^-	13^-
6515.7(4)	1336.2(3)	28(2)	1.05(7)	*B,D*	14^+	12^+	8897.9(6)	1410.4(3)	12(1)	1.04(6)	*B,F*	17^-	15^-
7858.3(6)	1342.6(4)	22(2)	1.12(8)	*B,D*	16^+	14^+	10430.3(8)	1532.4(4)	10(1)	1.06(8)	*B,F*	19^-	17^-
9305.8(7)	1447.5(4)	16(1)	1.10(4)	*B,D*	18^+	16^+	12088(1)	1658(1)	8.1(6)	1.08(11)	*B,F*	21^-	19^-
10881(1)	1575(1)	10(1)	1.05(5)	*C,D*	20^+	18^+	13896(2)	1808(1)	6.0(5)	1.18(23)	*E*	(23^-)	21^-
12650(2)	1769(1)	8.0(8)	0.98(7)	*C,D*	22^+	20^+	15907(2)	2011(1)	4.0(4)	1.04(20)	*B,F*	(25^-)	(23^-)
14687(2)	2037(1)	5.1(6)	1.07(10)	*C,D*	24^+	22^+	18172(2)	2265(1)	2.2(4)	1.20(26)	*B*	(27^-)	(25^-)
17067(2)	2380(1)	2.5(5)	1.17(24)	*B*	(26^+)	24^+	20734(3)	2562(2)	0.8(2)			(29^-)	(27^-)
19859(3)	2792(2)	1.0(2)			(28^+)	(26^+)							
							2655.7(3)	714.3(1)	6.1(3)	0.71(6)	*A,G*	$4^{(-)}$	$3^{(+)}$
1203.2(4)	747(1)	1.1(2)			(2^+)	2^+		1643(1)	0.4(1)			$4^{(-)}$	4^+
	1204(1)	1.5(5)	[b]		(2^+)	0^+	3139.0(2)	327.3(3)	1.5(2)	0.66(18)	*B*	$6^{(-)}$	5^-
1941.4(3)	738.3(3)	1.8(3)	0.58(16)	*I*	$3^{(+)}$	(2^+)		483.3(1)	5.8(3)	0.97(10)	*A,G*	$6^{(-)}$	$4^{(-)}$
	928(1)	1.1(2)			$3^{(+)}$	4^+		525.9(2)	6.8(4)	0.57(9)	*B,G*	$6^{(-)}$	$5^{(+)}$
	1486.0(5)	6.4(8)	0.84(7) [b]	*H,I*	$3^{(+)}$	2^+		1358(1)	1.9(3)			$6^{(-)}$	6^+
2613.0(2)	671.5(3)	2.3(3)	0.96(12)	*A,I*	$5^{(+)}$	$3^{(+)}$	3840.2(3)	387.9(5)	1.3(2)			$8^{(-)}$	(7^+)
	831(1)	0.5(2)			$5^{(+)}$	6^+		473.2(4)	1.0(2)			$8^{(-)}$	7^-
	1599.6(3)	4.6(5)	0.50(12)	*A,I*	$5^{(+)}$	4^+		701.3(2)	13(1)	1.01(7)	*B,H*	$8^{(-)}$	$6^{(-)}$
3452.4(4)	839.4(7)	1.2(2)			(7^+)	$5^{(+)}$	4721.2(4)	881.0(2)	12(1)	1.06(6)	*B,H*	$10^{(-)}$	$8^{(-)}$
	1671(1)	0.8(3)			(7^+)	6^+	5764.1(4)	1042.9(2)	11(1)	1.00(8)	*B,H*	$12^{(-)}$	$10^{(-)}$
4469(1)	1017(1)	0.6(2)				(7^+)	6967(1)	1203(1)	9.0(8)	1.00(9) [b]	*B,H*	$14^{(-)}$	$12^{(-)}$
5655(2)	1186(1)	0.4(1)					8318(1)	1351(1)	8.1(6)	1.09(11)	*B,H*	$16^{(-)}$	$14^{(-)}$
							9803(2)	1485(1)	6.0(8)	0.84(7) [b]	*H,I*	$18^{(-)}$	$16^{(-)}$
3761.3(8)	1980(1)	1.2(2)			8^+	6^+	11430(2)	1627(1)	4.8(4)	1.03(14)	*B,H*	$20^{(-)}$	$18^{(-)}$
4556.4(8)	795.2(6)	1.2(2)			10^+	8^+	13193(2)	1763(1)	3.0(2)	1.10(16)	*B,H*	$22^{(-)}$	$20^{(-)}$
	1809(2)	1.5(4)	[b]		10^+	8^+	15126(2)	1933(1)	1.7(2)			(24^-)	$22^{(-)}$
5570.3(7)	1014(1)	2.3(5)	0.99(16)	*B*	12^+	10^+	17299(3)	2173(2)	1.0(2)			(26^-)	(24^-)
	1678(1)	2.0(5)	[b]		12^+	10^+	19750(4)	2451(2)	0.4(1)			(28^-)	(26^-)
6853.1(8)	1283(1)	2.5(5)	[b]		14^+	12^+	3005.1(6)	1992(1)	1.6(2)			(5^-)	4^+
	1673(1)	5(1)	1.09(14)	*B,D*	14^+	12^+	3698.3(6)	693.3(3)	1.2(2)	0.91(23)	*B,J*	7^-	(5^-)
8412(1)	1559(1)	3.9(4)	1.08(33)	*A,D*	(16^+)	14^+		1917(1)	2.3(4)	0.45(9)	*B,J*	7^-	6^+
	1898(2)	0.9(2)			(16^+)	14^+	4592.2(6)	893.9(3)	3.6(3)	1.07(14)	*B,J*	9^-	7^-
9931(1)	2073(1)	2.4(3)	0.99(22)	*B*	(18^+)	16^+		1844(1)	0.5(1)			9^-	8^+
10135(2)	1723(1)	3.4(8)			(18^+)	(16^+)	5658.0(9)	1065.8(6)	4.0(4)	0.97(11)	*B,J*	11^-	9^-
11052(1)	1746(1)	2.2(3)				18^+	6874(1)	1216.2(8)	3.8(3)	0.96(16)	*B,J*	13^-	11^-
11985(2)	1850(1)	2.0(5)			(20^+)	(18^+)	8219(2)	1345(1)	2.7(3)			(15^-)	13^-
13925(3)	1940(2)	1.0(2)			(22^+)	(20^+)	9684(2)	1465(1)	2.2(3)			(17^-)	(15^-)
16010(3)	2085(2)	0.6(1)			(24^+)	(22^+)	11297(2)	1613(1)	1.8(3)			(19^-)	(17^-)
							13012(3)	1715(2)	1.3(2)			(21^-)	(19^-)
2811.7(3)	1799(1)	6.0(5)	0.65(10)	*B*	5^-	4^+	14828(4)	1816(2)	0.7(2)			(23^-)	(21^-)
3366.8(3)	555.1(2)	4.2(2)	[b]		7^-	5^-							

[a] *A*: 456 keV; *B*: 456+558 keV; *C*: 967+1144+1287+1336+1343 keV; *D*: 456+558+768 keV +*C*; *E*: 954+1124+1277+1410 keV; *F*: 767 keV+*E*; *G*: 701+881+1043+1203 keV; *H*: 483 keV+*G*; *I*: 456 keV+*H*; *J*: 456+558+894+1066 keV.
[b] Doublet structure.

TABLE IV. The energies of excited states in ^{78}Sr, the transitions energies and relative intensities of the γ rays placed in the level scheme, the DCO ratios and the gate used to obtain them, and the spins and parities of the initial and final states of the γ rays.

E_x (keV)	E_γ (keV)	I_{rel} (%)	R_{DCO}	Gate [a]	I_i^π ($\hbar$)	I_f^π ($\hbar$)	E_x (keV)	E_γ (keV)	I_{rel} (%)	R_{DCO}	Gate [a]	I_i^π ($\hbar$)	I_f^π ($\hbar$)
277.6(1)	277.6(1)	100(4)	1.03(4)	*E*	2^+	0^+	11428(4)	1558(3)	2(1)			(20^-)	(18^-)
780.8(1)	503.2(1)	100(3)	0.98(5)	*C*	4^+	2^+	2712(1)	1931(2)	3(1)	[c]		(5^-)	4^+
1493.2(2)	712.4(2)	84(3)	1.09(7)	*A*	6^+	4^+	3385.0(9)	673(1)	3(1)	1.03(25)	*A*	$7^{(-)}$	(5^-)
2388.4(3)	895.2(2)	68(2)	1.07(8)	*C*	8^+	6^+		1892(1)	6(1)	0.54(20)	*A*	$7^{(-)}$	6^+
3446.2(4)	1057.8(2)	52(2)	0.96(7)	*D*	10^+	8^+	4251.1(9)	866.1(3)	8(1)			(9^-)	$7^{(-)}$
4657.5(5)	1211.3(3)	43(2)	1.11(9) [c]	*D*	12^+	10^+		1862(2)	5(1)			(9^-)	8^+
6025.4(6)	1367.9(4)	31(2)	1.07(15)	*D*	14^+	12^+	5281(1)	1030.0(5)	10(1)			(11^-)	(9^-)
6035.8(9)	1378(1)	11(1)			14^+	12^+	6436(1)	1155.2(6)	9(1)			(13^-)	(11^-)
7559.0(7)	1523(1)	8(1)			16^+	14^+	7671(1)	1235.0(7)	8(1)			(15^-)	(13^-)
	1533.7(4)	21(1)	1.00(13)	*D*	16^+	14^+	8987(2)	1316(1)	7(1)			(17^-)	(15^-)
9253.7(9)	1694.7(5)	16(1)	1.00(19)	*D*	18^+	16^+	10448(2)	1461(1)	5(1)			(19^-)	(17^-)
10995(1)	1741(1)	8(1)			(20^+)	18^+	12109(3)	1661(2)	3(1)			(21^-)	(19^-)
11195(1)	1941(1)	6(1)	[c]		(20^+)	18^+							
12981(2)	1986(2)	5(1)			(22^+)	(20^+)	1903.3(7)	1626(1)	3(1)				2^+
13294(2)	2099(2)	3(1)			(22^+)	(20^+)	2310.4(8)	1530(1) [b]	3(1)	[c]		(3^-)	4^+
15233(4)	2252(3)	3(1)			(24^+)	(22^+)	2606.0(5)	703(1)	2(1)			$4^{(-)}$	
17764(6)	2531(4)	2(1)			(26^+)	(24^+)		1825.0(5)	11(1)	0.90(24)	*A*	$4^{(-)}$	4^+
							2860.1(5)	254.0(2)	7(1)	0.53(14)	*B*	$5^{(-)}$	$4^{(-)}$
1478(1)	1200(1)	3(1)				2^+		550(1)	2(1)			$5^{(-)}$	(3^-)
2244(1)	766(1)	2(1)						2080(2)	5(1)			$5^{(-)}$	4^+
3231(2)	987(1)	2(1)					3080.1(5)	219.8(3)	2(1)			(6^-)	$5^{(-)}$
								475(1)	2(1)			(6^-)	$4^{(-)}$
2537.1(7)	1756(1)	4(1)			(4^-)	4^+	3173.1(6)	313.0(4)	3(1)	0.48(15)	*A*	$6^{(-)}$	$5^{(-)}$
3138.9(8)	601.7(5)	4(1)			$6^{(-)}$	(4^-)		567(1)	2(1)			$6^{(-)}$	$4^{(-)}$
	1646(1)	6(1)	1.26(39)	*C*	$6^{(-)}$	6^+	3525.7(5)	352(1)	1(1)			(7^-)	$6^{(-)}$
3927.3(9)	788.4(5)	8(1)	1.16(27)	*C*	$8^{(-)}$	$6^{(-)}$		445.4(4)	2(1)			(7^-)	(6^-)
4883(1)	956.0(5)	8(1)			(10^-)	$8^{(-)}$		665.6(3)	6(1)			(7^-)	$5^{(-)}$
5982(1)	1098.7(6)	7(1)			(12^-)	(10^-)	3963.9(9)	438(1)	1(1)			(8^-)	(7^-)
7190(2)	1208(1)	6(1)	[c]		(14^-)	(12^-)		791(1)	2(1)			(8^-)	$6^{(-)}$
8474(2)	1284(1)	5(1)			(16^-)	(14^-)	4401(1)	875(1)	8(1)			(9^-)	(7^-)
9870(3)	1396(2)	4(1)			(18^-)	(16^-)	5469(2)	1068(1)	6(1)			(11^-)	(9^-)

[a] *A*: 278 keV; *B*: 278+504 keV; *C*: 278+712 keV; *D*: 278+712+895 keV; *E*: 504+712+895 keV, thick target run.
[b] Calculated from level energies.
[c] Doublet structure.

cially in the course of alignment processes, for which single protons and neutrons occupy the same high-j low-Ω $g_{9/2}$ orbitals. In such cases, the residual $T=0$ $(n\text{-}p)$ interaction may also influence the alignment pattern.

The present study is aimed at extending the yrast sequences beyond the first proton and neutron $g_{9/2}$ crossings and at identifying positive- and negative-parity sidebands. The bandhead energies provide a measure of the energy gaps in the Nilsson scheme. Since the level density is low, the bandhead configurations of excited bands most likely involve particles moving in the deformed $\mathcal{N}=3$ orbits originating from fp subshells. Thus, excited bands may provide further insight into the properties of the [301]3/2 or other similarly flat orbitals which may act as spectators and produce nearly ''identical'' bands [34].

The experimental procedures and the resulting level schemes are described in Sec. II. In Sec. III we shall compare the experimental band head energies, moments of inertia, band-crossing frequencies, and relative alignments with the predictions of cranked shell model calculations for the three $T_z=1$ nuclei studied in this work. For completeness, some aspects of the experimental level scheme for the odd-odd nucleus ^{76}Rb [35] that are relevant to this study will be presented also. The conclusions and a summary will be given in Sec. IV.

II. EXPERIMENTAL PROCEDURES AND RESULTS

The experiment was performed at the 88-Inch Cyclotron at the Lawrence Berkeley National Laboratory. High-spin states in the $T_z=1$ nuclei were populated via the reactions ^{58}Ni(^{28}Si,3α)^{74}Kr, ^{58}Ni(^{28}Si,2α)^{78}Sr, and ^{58}Ni(^{28}Si, $2p2n$)^{82}Zr at 130 MeV beam energy with an average beam intensity of 5 particle nA. The experimental setup included the Gammasphere array [36] then comprising 57 Compton-

TABLE V. The energies of excited states in ^{82}Zr, the transitions energies and relative intensities of the γ rays placed in the level scheme, the DCO ratios and the gate used to obtain them, and the spins and parities of the initial and final states of the γ rays.

E_x (keV)	E_γ (keV)	I_{rel} (%)	R_{DCO}	Gate [a]	I_i^π ($\hbar$)	I_f^π ($\hbar$)	E_x (keV)	E_γ (keV)	I_{rel} (%)	R_{DCO}	Gate [a]	I_i^π ($\hbar$)	I_f^π ($\hbar$)
407.0(1)	407.0(1)	120(4)	1.03(4) [b]	*B*	2^+	0^+	4973.1(9)	950.6(4)	4(1)			(10^-)	(8^-)
1040.8(1)	633.9(1)	100(3)	1.01(3) [c]	*A*	4^+	2^+	6100(1)	1127(1) [e]	3(1)			(12^-)	(10^-)
1887.9(2)	847.0(2)	76(2)	1.07(3)	*C*	6^+	4^+	7345(2)	1245(1)	2(1)			(14^-)	(12^-)
2908.6(4)	1020.7(3)	48(3)	1.15(6)	*D*	8^+	6^+							
4036.9(5)	1128.3(3)	39(2)	1.03(4) [e]	*D*	10^+	8^+	2791.6(3)	1750.7(3)	4(1)	0.46(11)	*B*	$5^{(-)}$	4^+
5213.4(7)	1176.5(4)	31(2)	1.03(4) [e]	*D*	12^+	10^+	3480.8(4)	689(1)	3(1)			$7^{(-)}$	$5^{(-)}$
6490.7(7)	1277.3(3)	22(1)	1.04(6) [e]	*D*	14^+	12^+		1593.0(3) [e]	8(1)	0.67(17)	*C* [b]	$7^{(-)}$	6^+
7859.6(8)	1368.9(4)	15(1)	1.02(13) [e]	*D*	16^+	14^+	4347.7(5)	866.9(3)	9(1)	1.07(12)	*C*	$9^{(-)}$	$7^{(-)}$
7992(1)	1502(1)	3(1)			(16^+)	14^+		1439(1)	4(1)			$8^{(-)}$	8^+
9112(1)	1252(1)	7(1)	1.10(16)	*D*	18^+	16^+	5361.4(8)	1013.7(6)	11(1)	1.00(14)	*C*	$11^{(-)}$	$10^{(-)}$
9453(1)	1461(2)	2(1)			(18^+)	(16^+)	6536(1)	1174.4(7)	10(1)	[e]		$13^{(-)}$	$11^{(-)}$
	1593(1) [e]	3(1)			(18^+)	16^+	7688(2)	1152(1)	3(1)			(15^-)	$13^{(-)}$
10491(2)	1379(1)	4(1)			(20^+)	18^+	7908(2)	1372(2)	3(1)	[e]		(15^-)	$13^{(-)}$
12127(2)	1636(1)	3(1)			(22^+)	(20^+)	9047(3)	1359(1)	2(1)			(17^-)	(15^-)
14013(3)	1886(2)	2(1)			(24^+)	(22^+)	9235(3)	1327(1)	2(1)			(17^-)	(15^-)
16120(5)	2107(3)	1(1)			(26^+)	(24^+)							
							2057.3(6)	1017(1) [e]	3(1)				4^+
1060.8(2)	653.8(2)	4(1)				2^+	2857.0(2)	800(1)	1(1)			5^-	
1449.1(2)	387.7(6)	3(1)			$(3)^+$			1816.1(2)	9(1)	0.47(7)	*B*	5^-	4^+
	408.3(3) [d,e]	1.0(5)			$(3)^+$	4^+	3128.1(3)	271.1(2)	7(1)	0.53(5)	*B*	6^-	5^-
	1041.7(3)	7(1)	0.85(9) [c]	*A*	$(3)^+$	2^+		336.6(3)	1(1)			6^-	$5^{(-)}$
2175.4(3)	726.0(2)	10(1)	0.95(12)	*A*	$(5)^+$	$(3)^+$		1071(1) [e]	2(1)			6^-	
	1135.2(3)	5(1)			$(5)^+$	4^+	3506.8(4)	377.5(6)	3(1)	0.43(7)	*B*	7^-	6^-
3068.4(4)	893.1(3)	14(1)	0.93(7)	*C*	$(7)^+$	$(5)^+$		650.1(4)	3(1)			7^-	5^-
	1180(1) [d,e]	3(1)			$(7)^+$	6^+		1619(2)	1(1)			7^-	6^+
4086.3(6)	1017.9(4)	12(2)	[e]		$(9)^+$	$(7)^+$	3946.7(4)	439.2(7)	2(1)			8^-	7^-
5195(1)	1109(1)	10(2)	0.94(13) [e]	*C*	$(11)^+$	$(9)^+$		818.7(3)	8(1)	1.07(9)	*B*	8^-	6^-
6406(2)	1211(1)	7(1)			(13^+)	$(11)^+$	4444.1(8)	937(1)	3(1)			(9^-)	7^-
7680(2)	1274(1)	3(1)	[e]		(15^+)	(13^+)	4908.3(6)	464(1)	1(1)			10^-	(9^-)
7750(2)	1344(1)	3(1)			(15^+)	(13^+)		961.7(4)	8(1)	1.07(10)	*B*	10^-	8^-
9070(3)	1390(2)	2(1)			(17^+)	(15^+)	5550(2)	1106(2)	2(1)	[e]		(11^-)	(9^-)
9183(3)	1433(2)	2(1)			(17^+)	(15^+)	5989.1(8)	1080.8(5)	8(1)	1.21(19)	*C*	12^-	10^-
							7041.6(9)	1052.5(5)	6(1)	0.99(20)	*C*	14^-	12^-
2691.5(8)	1651(1)	1(1)			(4^-)	4^+	8114(1)	1072(1)	5(1)	1.01(16) [e]	*C*	16^-	14^-
3287.2(7)	219(1)	1(1)			(6^-)	$(7)^+$	9339(2)	1225(1)	4(1)			(18^-)	16^-
	596(1)	1(1)			(6^-)	(4^-)	10753(2)	1414(1)	3(1)			(20^-)	(18^-)
	1399(1)	6(1)			(6^-)	6^+	12365(3)	1612(2)	2(1)			(22^-)	(20^-)
4022.4(8)	735.3(4)	5(1)	0.92(17)	*C*	(8^-)	(6^-)							

[a] *A*: 407 keV; *B*: 634 keV; *C*: 407+634 keV; *D*: 407+634+847 keV.
[b] Result from backed target run.
[c] Mean value from thin and backed target run.
[d] Calculated from level energies.
[e] Doublet structure.

suppressed Ge detectors, and the 4π charged-particle detector array Microball, which consists of 95 CsI(Tl) scintillators with photodiode read-out [37]. The 57 Ge detectors were arranged in rings at 31.7° (5 detectors), 37.4° (5), 50.1° (9), 79.2° (1), 80.7° (1), 90.0° (5), 99.3° (1), 100.8° (1), 121.7° (5), 129.9° (10), 142.6° (5), 148.3° (4), and 162.7° (5). The event trigger required three or more Ge detectors firing. In 4 days of beam time 1.3×10^9 events were collected with a 99.7% enriched, 330 μg/cm^2 thin self-supporting ^{58}Ni target foil. In the final two shifts, a backed target, consisting of a 420 μg/cm^2 layer of ^{58}Ni evaporated onto a 10.5 mg/cm^2 thick Ta foil, was used to accumulate some 3.0×10^8 events. Due to the much larger amount of secondary electrons originating from the thick target, the counting rates of the individual Microball elements increased from about 4000 to 6000 counts per s, even though the beam intensity was reduced by a factor of 2. This enhanced background radiation led to a worse charged-particle identification, but in the

course of the off-line analysis we found the performance of Microball still reasonable and at least helpful in terms of reaction-channel selection. At the end of the experiment, the Ge detectors were energy and efficiency calibrated with ^{56}Co and ^{152}Eu sources.

The events were sorted off line into various E_γ-E_γ matrices and E_γ-E_γ-E_γ cubes subject to the appropriate charged-particle and analysis conditions. A summary is presented in Table I. Proton and alpha particles were identified and cleanly separated using two independent pulse-shape discrimination techniques [37]. The efficiency of the whole detection and trigger system, including a restrictive off-line procedure for clean particle identification, was found to be 78(1)% for protons and 63(2)% for α particles in this experiment. The reduced efficiency for the α particles is mainly due to the absorbers in front of the Microball detectors. In addition to the exit-channel selection, the Microball data were used to determine the momenta of the recoiling residual nucleus from an event-by-event evaluation of the momenta of all emitted charged particles. This allowed a precise Doppler-shift correction to be made and considerably improved the overall γ-ray energy resolution. The $2p$ and 2α gates contained sizable admixtures of higher charged-particle folds ($3p$, $4p$, $\alpha 2p$, $\alpha 3p$, $2\alpha 2p$, and $2\alpha p$, $2\alpha 2p$, 3α, respectively) which leaked through when one or two protons or α particles escaped detection.

Table II shows the experimental relative cross sections for the reaction ^{28}Si+^{58}Ni which are deduced from the yields of known ground-state and bandhead transitions in various spectra with different charged-particle gating conditions. Because of the energy loss in the target foil, the mean beam energy is approximately 128 MeV. The large number ($\approx$30) of detectable reaction channels requires the use of Microball for the selection of weak channels or structures such as superdeformed bands or excited states in $N\approx Z$ nuclei. Due to the high beam energy, the number of evaporated particles per event is approximately four. The raw γ-ray spectra are dominated by the pure charged-particle channels ^{79}Rb+$\alpha 3p$, ^{80}Sr+$\alpha 2p$, and ^{82}Sr+$4p$. Double-α evaporation channels such as ^{77}Rb and ^{76}Kr are also comparatively strong ($\approx$5% of the total fusion cross section) and are similar to the multi-proton one-neutron channels (^{82}Y+$3pn$, ^{81}Sr+$4pn$, ^{79}Sr+$\alpha 2pn$). The relative yields of the even-even $T_z=1$ nuclei are $\approx$0.5% and provide enough statistics in this experiment to deduce extensive level schemes. The relative cross sections leading to the $N=Z$ nuclei ^{80}Zr and ^{76}Sr are too small to provide considerable new information. A perfect (100% detection efficiency and no misidentification) $1\alpha 0p$ particle gate should contain almost exclusively transitions from the reaction channel ^{80}Zr + $\alpha 2n$. In this experiment, however, only a coincidence relationship between the two known γ rays [38] and two candidates for the $6^+\rightarrow 4^+$ transition at 770 or 792 keV could be found. The leak through from other reaction channels due to the escaped protons and α particles was overwhelming. For example, the transitions from ^{80}Sr are a factor of $\approx$250 more intense than those of ^{80}Zr in the $1\alpha 0p$ gated spectra. Even if the detection efficiency for protons were to be 95%, this factor would be $\approx$10.

The geometry of the Gammasphere also allowed the assignments of spins based on the angular correlations of the γ rays. For this purpose matrices were constructed in which γ events recorded between 80° and 100° were sorted against those recorded at 31.7°, 37.4°, 142.6°, 148.3°, or 162.7° in coincidence with the appropriate charged particles (see Table I) detected in Microball. The inclusion of Ge detectors at nearly the same angles does not significantly affect the analysis. The cosines of the detector angles around 90° average to the cosine of an angle at 86° and those of the latter five angles to the cosine of 32° (the angular distribution of γ rays following heavy ion fusion evaporation reactions is symmetric with respect to 90°). Pairs of gated spectra may be used to obtain directional correlations of oriented states (DCO ratios), defined as

$$R_{\mathrm{DCO}}(\gamma_1,\gamma_2)=\frac{I(\gamma_1 \text{ at } 32^\circ;\ \text{gated with } \gamma_2 \text{ at } 86^\circ)}{I(\gamma_1 \text{ at } 86^\circ;\ \text{gated with } \gamma_2 \text{ at } 32^\circ)}, \tag{1}$$

where γ_2 is a stretched $E2$ transition. The DCO ratios were not corrected for detection efficiency because the relative efficiency of the detectors at ''32°'' and ''86°'' were found to be equal within the 3% accuracy of the efficiency calibration. The DCO ratios obtained are given in Tables III–V together with the corresponding gates. In most cases gates were summed up in order to improve statistics. This procedure does not significantly affect the results as shown in Ref. [39]. The expected DCO ratios are $R_{\mathrm{DCO}}=1.0$ for a stretched $E2$ transition and $R_{\mathrm{DCO}}\approx 0.5$–$0.6$ for a stretched dipole transition. Depending on the multipole mixing ratio $\delta(E2/M1)$, the DCO ratio may differ from these values. Matrices were generated for both the thin and the thick target experiments. The thick-target data were especially helpful in determining the DCO ratios and, hence, multipolarities of the interband transitions between the sidebands and the positive-parity yrast cascades. Since the lifetimes of these states are typically on the order of picoseconds, the corresponding γ rays are emitted when the recoiling nuclei are at rest. This leads to clean sharp lines in the spectra which here allow for a proper analysis despite a decrease of the overall statistics.

The spin assignments are also based on intensity arguments; i.e., the more intense a band or transition is the closer to the yrast line it is supposed to be. If the transitions are too weak to deduce DCO ratios, $E2$ character is tentatively assigned to the transitions on top of rotational bands. High-energy (1.5–2.0 MeV) $\Delta I=1$ transitions with magnetic dipole character contain most likely a sizable amount of electric quadrupole radiation. Thus the DCO ratios defined in Eq. (1) lie between the values presented for pure stretched dipole and pure stretched quadrupole radiation. However, parity changing electric dipole transitions are expected to be pure in the γ-ray energy range considered. Therefore, $\Delta I=1$ $E1$ character has been attributed if the DCO ratios of high-energy γ rays depopulating bandheads were consistent with $R_{\mathrm{DCO}}\approx 0.55$ and their uncertainties were less than some 20%. Otherwise, the parities (and spins) of the corresponding level have been placed in parantheses.

The more extensive studies with the large γ-detector arrays such as Eurogam or Gammasphere have revealed more and more forkings at high rotational frequencies. Therefore, distinct coincidence relationships between the two highest lying transitions are demanded for building the level scheme.

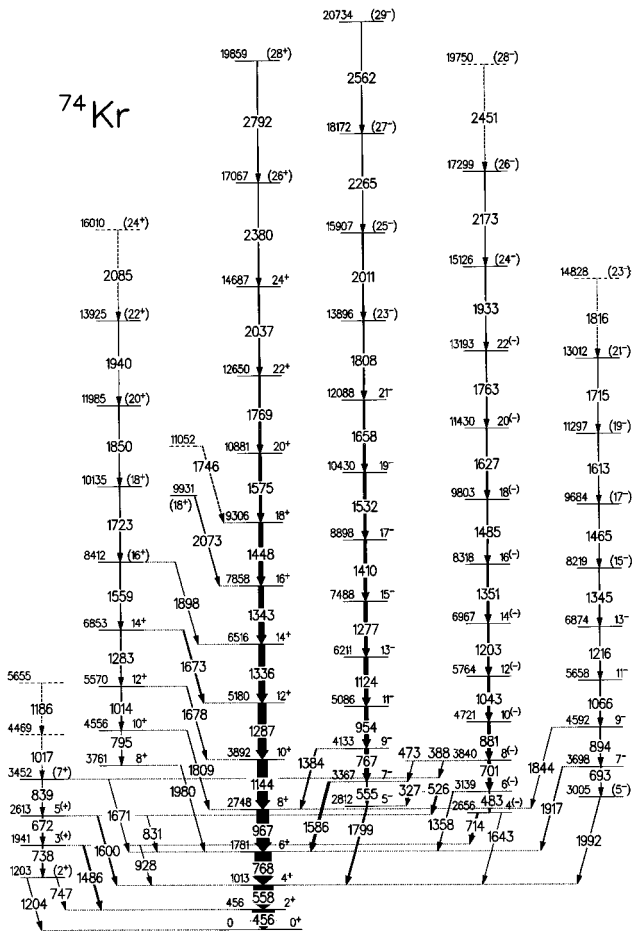

FIG. 1. Proposed partial level scheme of ^{74}Kr. The energy labels are given in keV. The widths of the arrows are proportional to the relative intensities of the γ rays. Tentative transitions and levels are dashed.

Otherwise, the transitions are dashed and tentatively placed on top of the bands based on the expected increase of γ-ray energies in rotational bands (e.g., the transitions with 1816, 2085, and 2451 keV in Fig. 1).

A. Experimental results for ^{74}Kr

Excited states in ^{74}Kr were first observed by Piercey *et al.* [40] up to the $I^{\pi}=8^{+}$ state. The level scheme was extended by Roth *et al.* [41], who also measured lifetimes of the first two excited states using the recoil distance Doppler shift (RDDS) technique. The yrast states above the 10^{+} state and the sidebands were corrected and extended in studies of Tabor *et al.* [20] and Heese *et al.* [21]. They presented consistent level schemes up to a tentative 20^{+} level at 11 MeV excitation energy, the beginnnings of two negative-parity bands, as well as lifetimes in the yrast band measured with the Doppler shift attenuation (DSA) method. The major findings were a prolate-oblate shape coexistence at low spins (2^{+}, 4^{+} levels, see also [7]), and a simultaneous proton and neutron $g_{9/2}$ band crossing at a rotational frequency of $\hbar\omega=0.66$ MeV in the strongly deformed prolate ($\beta_2\approx 0.4$) positive-parity yrast cascade.

The level scheme of ^{74}Kr deduced from the present work is presented in Fig. 1 and summarized in Table III. The

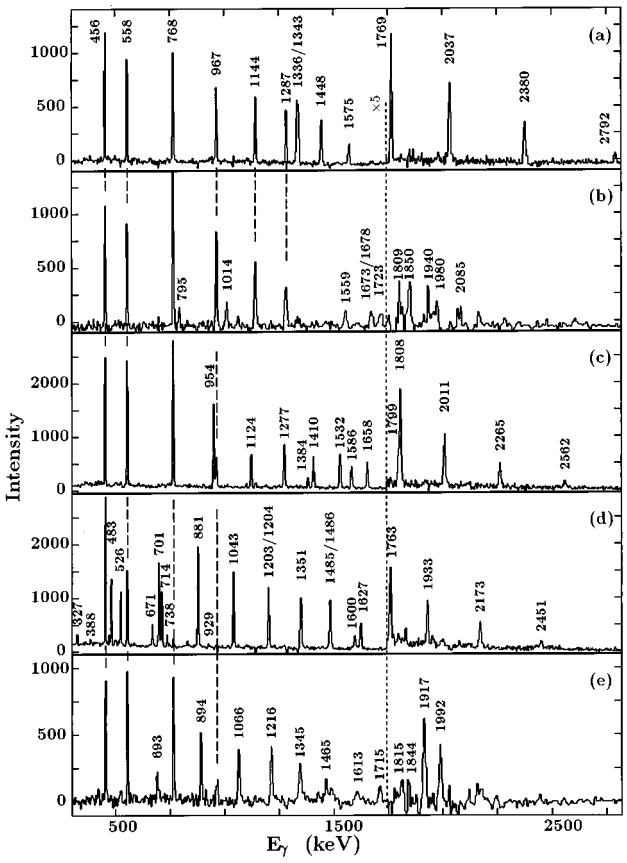

FIG. 2. Coincidence spectra of ^{74}Kr: (a) sum of the spectra in coincidence with the 1575, 1769, 2037, and 2380 keV transitions ($\pi=+$, $\alpha=0$ yrast band) in the 3α-gated $\gamma\gamma$ matrix; (b) sum of double-gated spectra in the 2- or 3α-gated cube with one gate being the 456 or 558 keV transition and the second the 795, 1014, 1559, 1673, 1678, 1723, or 1850 keV transition ($\pi=+$, $\alpha=0$ yrare band); (c) sum of spectra in coincidence with the 1124, 1277, and 1410 keV transitions ($\pi=-$, $\alpha=1$ yrast band) in the 3α-gated $\gamma\gamma$ matrix; (d) sum of spectra in coincidence with the 483, 701, 1043, 1203, and 1485 keV transitions ($\pi=-$, $\alpha=0$ yrast band) in the 3α-gated $\gamma\gamma$ matrix; and (e) sum of double-gated spectra in the 2- or 3α-gated cube with one gate being the 456 or 558 keV transition and the second the 793, 894, 1066, 1216, 1917, or 1992 keV transition ($\pi=-$, $\alpha=1$ yrare band). The energy labels are given in keV.

positive-parity yrast sequence was extended to a likely spin $I^{\pi}=28^{+}$ at 20 MeV excitation energy. The previously reported high-spin scheme [20,21] was confirmed with the exception of the tentative 1560 keV $20^{+}\rightarrow 18^{+}$ transition [21], which is assigned to be 1575 keV in this work. The negative-parity yrast bands reach spins of $I^{\pi}=28^{-}$ and 29^{-} at 20 and 21 MeV excitation energy, respectively. These values are amongst the highest observed for normally deformed bands in this mass region [19,26]. In the bandhead region of the $\pi=-$, signature $\alpha=0$ band, a few of the previously tentative spin assignments were changed. Therefore, only new levels in the known cascades and the three rotational bands observed will be discussed in the following.

Figure 2 shows γ-ray spectra for the ^{74}Kr+3α reaction channel obtained by summing up a number of spectra subject to different gating conditions. Figure 2(a) is the sum of spectra in coincidence with the 1575, 1769, 2037, and 2380 keV

transitions in the 3α-gated $\gamma\gamma$ matrix. It illustrates the positive-parity yrast sequence and, especially in view of the peak at 2792 keV, the extremely good peak to background ratio that results from 3α-particle gating and kinematic correction. Figures 2(c) and 2(d) show the two signatures of the negative-parity yrast band. The gating conditions can be found in the figure caption. Figures 2(b) and 2(e) illustrate the new positive- and negative-parity yrare bands via sums of doubly gated spectra in a $\gamma\gamma\gamma$ cube gated with two or three α particles. The γ gate on one axis was used to select ^{74}Kr (456 or 558 keV), while a second gate selected the band to be displayed. The peak to background ratio becomes somewhat worse but the in-band and high-energy interband transitions [e.g., the 1917 and 1992 keV transitions in Fig. 2(e)] can clearly be seen and attributed to ^{74}Kr. The transitions connecting the various bands to the main positive-parity yrast band and their characteristics (energies, intensities, multipolarities) can also be nicely deduced from the thick-target experiment. In general, the recoiling nuclei are at rest by the time the γ cascade reaches the bandhead region. Hence, the lines in the spectra belonging to transitions depopulating these states are sharp whereas those of comparable γ-ray energy at the top of the bands have Doppler-broadened and Doppler-shifted line shapes.

The DCO ratios of the 1586 keV $7^- \rightarrow 6^+$ [$R_{\mathrm{DCO}}=0.56(5)$] and 1384 keV $9^- \rightarrow 8^+$ [$R_{\mathrm{DCO}}=0.57(10)$] transitions were used to fix the spins and parities of the yrast $(\pi,\alpha)=(-,1)$ band. The same argument holds for the 1917 keV $7^- \rightarrow 6^+$ transition for the yrare $(-,1)$ band. Based on systematics and intensity arguments, the level at 1203 keV is most likely the first excited 2^+ state. Neither the 747 nor the 1204 keV transition is intense enough to deduce DCO ratios. The DCO ratio of the 738 keV transition provides evidence for a spin $I=3$ for the 1941 keV level and the abnormally large DCO ratio of the 1486 keV transition (for a dipole transition) suggests positive parity for that level. The 1486 keV transition is a (self-coincident) doublet with the 1485 keV transition in the $(-,0)$ yrast band. However, the thick-target experiment confirmed the relatively large DCO ratio of the low lying $3^{(+)} \rightarrow 2^+$ transition. The DCO ratios of the 672 and 1600 keV transitions determine the spin and parity of the 2613 keV $5^{(+)}$ state, and those of the 714, 526, 483, and 327 keV transitions allow us to determine the spins of the 2656 ($I=4$) and 3139 keV ($I=6$) levels. With the present more complete information, the spins of the the 2613 and 2656 keV levels had to be interchanged with respect to Refs. [20,21], even though the DCO ratios of the 483 and 526 keV transitions in Table III agree with those given in Ref. [20]. The parity of these levels and the band cannot be rigorously determined on the basis of the available data. The pattern of the whole band, however, strongly favors it to be the signature partner of the yrast $(-,1)$ band. The spin and parity of the yrare $(+,0)$ band is determined by the DCO ratio of the 1673 keV $14^+ \rightarrow 12^+$ transition. All transitions in the yrast $(+,0)$ band have $E2$ character and because the same number of transitions exist in both bands between the yrare 14^+ and yrast 6^+ states, the transitions below the 6853 keV 14^+ state in the yrare band must also have $E2$ character.

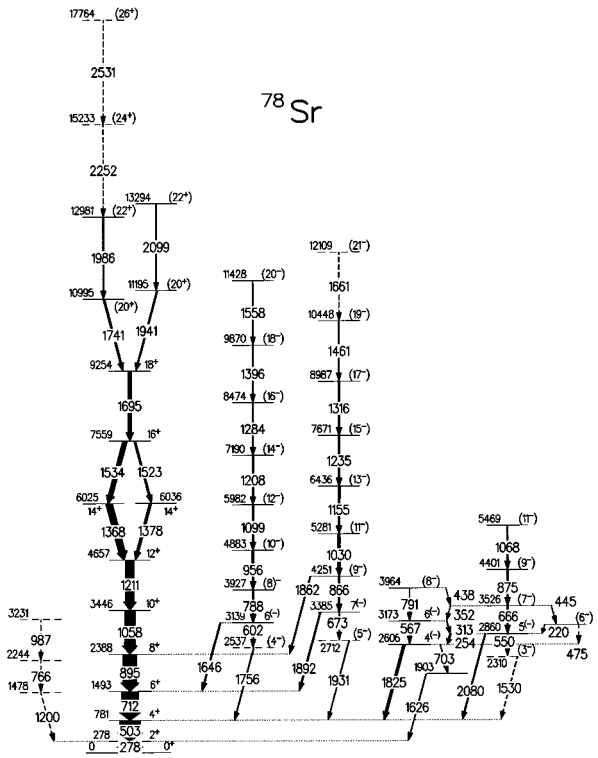

FIG. 3. Proposed partial level scheme of ^{78}Sr. The energy labels are given in keV. The widths of the arrows are proportional to the relative intensities of the γ rays. Tentative transitions and levels are dashed.

B. Experimental results for ^{78}Sr

Lister *et al.* [10] reported the positive-parity yrast cascade in ^{78}Sr up to the 10^+ state. Their measurement of the lifetimes of the first two excited states (RDDS) indicate $E2$ transition strengths of more than 100 Weisskopf units. Gross *et al.* [42,34] extended this sequence up to a tentative spin of $I^\pi=22^+$, but neither positive- nor negative-parity side bands were established. A band crossing was observed at $\hbar\omega \approx 0.55$ MeV, and two (or more) bands in ^{78}Sr seem to interact strongly and over a large range of frequencies, which is rather unsusual for this mass region. The cascade in ^{78}Sr was found to be identical to the negative-parity bands in ^{77}Sr and, partly, the high-spin part of the band built upon the 4^- state in ^{78}Rb [34]. This strongly suggested that the [301]3/2 Nilsson orbital acts as a spectator in the negative-parity bands.

Figure 3 shows the largely extended level scheme of ^{78}Sr from the present work. The data are compiled in Table IV. The known level scheme of ^{78}Sr [10,42,34] has essentially been confirmed. The 1941 keV (1939 keV in Ref. [34]) transition was found to be in coincidence with all the transitions in the yrast $(+,0)$ band with the exception of the 1741 keV transition. Hence, a forking is observed at high excitation energies. The situation is illustrated in Fig. 4. The spectra in Figs. 4 are the sums of doubly gated spectra in a 2α-gated $\gamma\gamma\gamma$ cube. In Fig. 4(a) one γ gate selects the $(+,0)$ yrast band below the 9254 keV 18^+ state, and the second γ gate selects the left part of the forking in Fig. 3 (the 503 keV $4^+ \rightarrow 2^+$ transition was excluded because it is a doublet with the strong 502 keV $13/2^+ \rightarrow 9/2^+$ transition in the

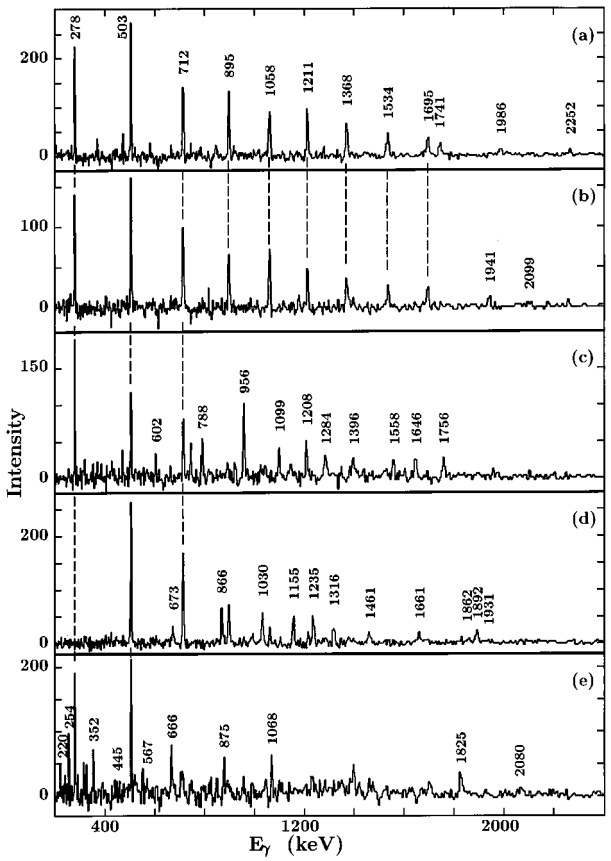

FIG. 4. Coincidence spectra of ^{78}Sr: (a) sum of double-gated spectra in the 2α-gated cube with one gate being the 278, 712, 895, 1058, 1211, 1368, 1534 or 1695 keV transition and the second the 1741, 1986, or 2252 keV transition; (b) same as (a) but the second gate being the 1941 or 2099 keV transition (both $\pi=+$, $\alpha=0$ bands); (c) sum of double-gated spectra in the 2α-gated cube with one gate being the 278, 503, or 712 keV transition and the second the 602, 788, or 956 keV transition ($\pi=-$, $\alpha=0$ yrast band); (d) sum of double-gated spectra in the 2α-gated cube with one gate being the 278 keV transition and the second the 673, 866, 1030, 1155, 1235, 1316, 1461, 1892, or 1931 keV transition ($\pi=-$, $\alpha=1$ yrast band); and (e) sum of double-gated spectra in the 2 α-gated cube with one gate being the 278 or 503 keV transition and the second the 220, 254, 313, 352, 445. 567, 666, 875, 1068, 1825, or 2080 keV transition ($\pi=-$ yrare bands).

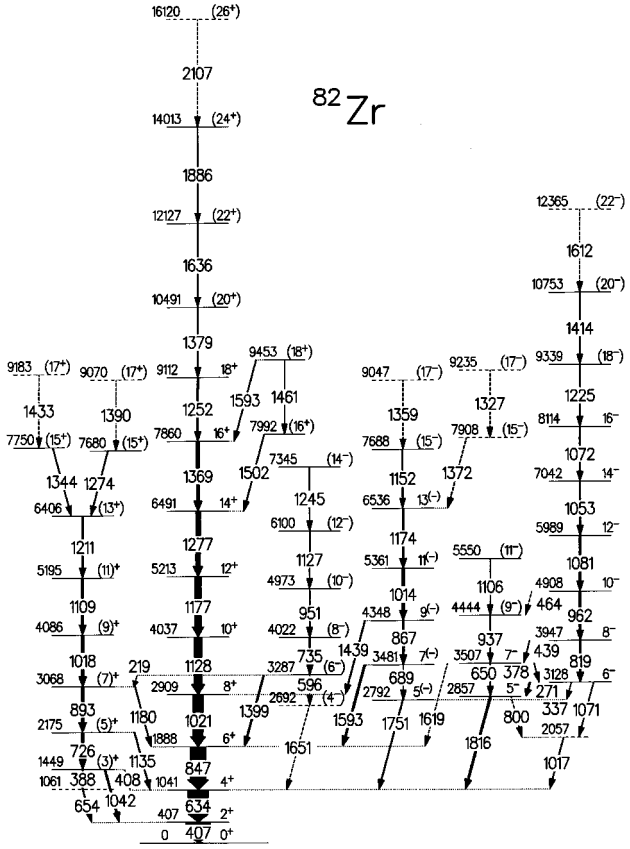

FIG. 5. Proposed partial level scheme of ^{82}Zr. The energy labels are given in keV. The widths of the arrows are proportional to the relative intensities of the γ rays. Tentative transitions and levels are dashed.

$2\alpha p$ channel ^{77}Rb [16,26]). In Fig. 4(b) the right branch was used for the second γ gate. Clearly, the 1741 and 1941 keV transitions are not in coincidence. The coincidence between the 1986 and 2252 keV transitions cannot be proven. Hence, the transitions on top of the 12981 keV level are tentative. The 2099 keV transition in the right branch was confirmed by means of γ-gated spectra from the 2α-gated $\gamma\gamma$ matrix. Another new feature in the (+,0) sequence is the existence of a second 14^+ level only 11 keV above the yrast level. There are some indications for the presence of a 1585 keV transition feeding into the yrare 14^+ level. However, our search failed to find possible links to the 11 195 keV (20^+) state.

According to its DCO ratio the character of the 1892 keV transition is most likely $E1$. However, the large uncertainty would also allow a mixed $E2/M1$ radiation for this transition. Thus the 3385 keV level is assigned to have a spin $I=7$ and most likely negative parity. The DCO ratio of the 1646 keV transition is consistent with either a $\Delta I=0$ or $\Delta I=2$ transition. Assuming the latter, the 5982 keV and all higher lying levels in this band would be yrast. This would, however, disagree with the observed intensities and the level sequence of this band strongly suggests it to be the signature partner of the previously mentioned negative-parity band. Figures 4(c) and 4(d) illustrate these two bands. Figure 4(e) shows the structure placed on the right-hand side of Fig. 3. The DCO ratio of the 1825 keV transition is consistent with a $\Delta I=0$ transition, and according to intensity arguments the 2606 keV state must have a spin of $I=4$. The presence of the interconnecting $\Delta I=1$ (see Table IV) with parallel $E2$ transitions in conjunction with the absence of strong signature splitting again favors negative parity for this weakly populated sequence.

Finally, a tentative cascade was found that feeds into the 278 keV 2^+ state (left-hand side of Fig. 3). In terms of γ-ray energies it might correspond to a $5^+\rightarrow 3^+ \rightarrow 2^+\rightarrow 2^+$ cascade similar to the ones in ^{74}Kr (Fig. 1), ^{82}Zr (Fig. 5) and other even-even isotopes in the region [15,43].

C. Experimental results for ^{82}Zr

In an early study, the 2^+, 4^+, and 6^+ states in ^{82}Zr were tentatively identified [44] and confirmed by Mitarai *et al.* [45]. They extended the positive-parity band up to a tentative spin of $I^\pi=20^+$ and reported one tentative side band. Dis-

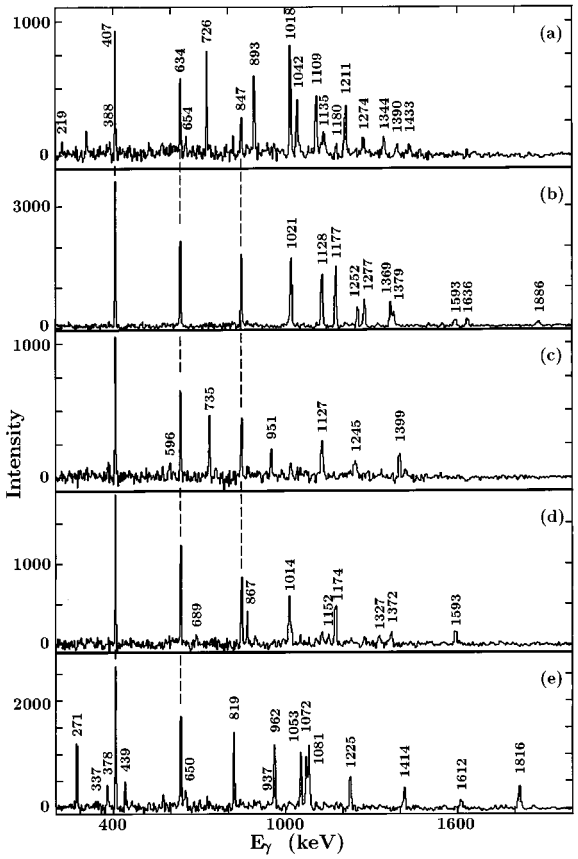

FIG. 6. Coincidence spectra of ^{82}Zr: (a) sum of double-gated spectra in the $2p$-gated cube with one gate being the 407 or 634 keV transition and the second the 726, 893, 1042, 1109, or 1211 keV transition ($\pi=+$, $\alpha=1$ yrast band); (b) sum of double-gated spectra in the $2p$-gated cube with one gate being the 407, 634, or 847 keV transition and the second the 1252, 1277, 1369, 1379, or 1636 keV transition ($\pi=+$, $\alpha=0$ yrast band); (c) same as (b) but the second gate being the 735, 951, or 1399 keV transition ($\pi=-$, $\alpha=0$ yrare band); (d) same as (b) but the second gate being the 689, 867, 1439, 1593, or 1751 keV transition ($\pi=-$, $\alpha=1$ yrast band); and (e) same as (a) but the second gate being the 271, 378, 650, 819, 962, 1053, 1072, 1081, 1225, or 1816 keV transition ($\pi=-$, $\alpha=0$ yrast band). The energy labels are given in keV.

tinct band crossings were observed at $\hbar\omega=0.57$ MeV and $\hbar\omega=0.69$ MeV and attributed to consecutive proton and neutron $g_{9/2}$ alignments. Finally, Chishti *et al.* [46] measured the lifetimes (RDDS) of the first two excited states. Both the rotationallike sequence of states and the transition strengths indicate a deformed ($\beta_2\approx0.3$) shape.

In Fig. 5 the level scheme of ^{82}Zr as deduced from the present work is presented and a summary can be found in Table V. The level scheme is consistent with the previous work up to the 7860 keV 16^+ state and the tentative sideband [45] has been confirmed. The reported 1375 keV $(18^+)\rightarrow(16^+)$ and tentative 1592 keV $(20^+)\rightarrow(18^+)$ transitions were found to belong to ^{82}Zr. However, a 1252 keV transition replaced the 1375 keV transition which is now placed as a 1379 keV transition on top of the 9112 keV 18^+ state. The 1593 keV γ ray is a doublet. With about 2/3 of its intensity carried by a new $7^{(-)}\rightarrow 6^+$ transition, it also is in coincidence with higher lying transitions in the yrast

TABLE VI. Lifetimes, transition strengths, quadrupole moments, and deformation parameters in the axial symmetric limit for positive-parity yrast states in ^{82}Zr.

E_x (keV)	I_i^π ($\hbar$)	E_γ (keV)	τ (ps)	$B(E2)$ (e^2 fm^4)	$\lvert Q_t\rvert$ (e b)	$\lvert\beta_2\rvert$
6491	14^+	1277	$<0.39^a$	>610	>1.32	>0.15
5213	12^+	1177	0.19(6)	$1910(^{910}_{470})$	$2.36(^{51}_{31})$	0.26(5)
4037	10^+	1128	0.23(6)	$1940(^{710}_{420})$	$2.40(^{41}_{27})$	0.27(4)
2909	8^+	1021	0.32(8)	$2300(^{800}_{480})$	$2.65(^{43}_{29})$	0.29(4)
1041	4^+	634	$<10^{a,b}$	>790	>1.67	>0.19
407	2^+	407	40(4) [b]	$1830(^{220}_{180})$	$3.03(^{18}_{16})$	0.33(2)

[a]Effective lifetime not corrected for feeding.
[b]From Ref. [46].

(+,0) band including the 1369 keV $16^+\rightarrow 14^+$ transition. The construction of the new ^{82}Zr level scheme is mainly based on the analysis of the $2p$-gated $\gamma\gamma\gamma$ cube. Since only a few percent of the raw $2p$-gated events originate from ^{82}Zr, the $2p$-gated $\gamma\gamma$ matrices contained many strong contaminating transitions. Fortunately, the first three transitions (407, 634, and 847 keV) in the main (+,0) yrast band were found to be essentially clean. For example, only weak transitions in ^{82}Sr+$4p$ (409 keV $18^+\rightarrow 17^+$) and ^{79}Rb+$\alpha 3p$ (407 keV $13/2^-\rightarrow 11/2^-$) contaminated the 407 keV gate of ^{82}Zr. Depending on the part of the ^{82}Zr level scheme to be analyzed, these first two or first three transitions were used to select ^{82}Zr in the $2p$-gated $\gamma\gamma\gamma$ cube. The second γ gate to be applied was then taken from transitions within the various bands shown in Fig. 5.

Figure 6 illustrates sums of doubly gated spectra in the $2p$-gated cube prepared with the procedure described above. Figure 6(b) presents the positive-parity yrast sequences which was extended up to a probable spin of $I^\pi=26$ at 16 MeV excitation energy. Definite spin assignments were possible up to the 9112 keV 18^+ level. The yrare states at 7992 and 9453 keV may represent the continuation of the 2 quasiparticle (qp) band. On the left-hand side of Fig. 5 and in Fig. 6(a), the previously tentatively (1042, 726, and 893 keV) assigned side band is shown. Similar to the 1486 keV transition in ^{74}Kr, the DCO ratio of the 1042 keV transition lies in between the expected values for pure $\Delta I=1$ and $\Delta I=2$ transitions [$R_{\rm DCO}=0.85(9)$] for both the thin- and the backed-target runs. This DCO ratio excludes a parity-changing $E1$ $\Delta I=1$ character and an $E1$ $\Delta I=0$ assignment is unlikely in terms of the DCO ratio, systematics, and intensity arguments. The band is significantly more intense than the structure built upon the 2692 keV (4^-) state. Finally, the existence of the 408 keV transition rules out a 2^- assignment for the 1449 keV level. The intensity argument also favors a $\Delta I=1$ assignment, but $\Delta I=0$ cannot be ruled out completely. Therefore, the spin-parity assignment of the 1449 keV state is $I^\pi=(3)^+$. Similar to the neighboring even-even nuclei the level at 1061 keV most likely represents the first excited 2^+ state.

Figures 6(c) and 6(d) show the two bands in the middle of the level scheme of Fig. 5. Arguments similar to those in the cases of ^{74}Kr and ^{78}Sr may be used to assign the spins and a tentative negative parity. For the structure on the right-hand side of Fig. 5 the DCO ratio of the 1816 keV transition

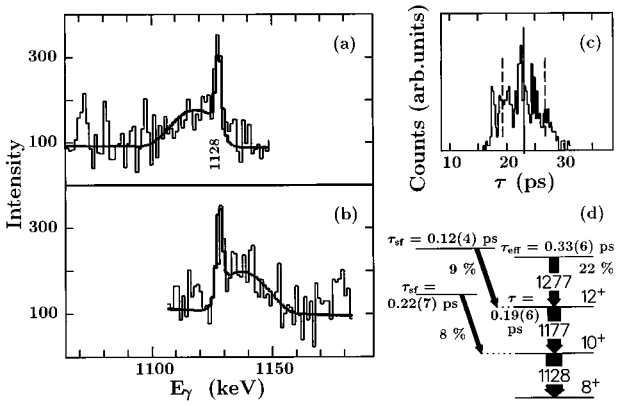

FIG. 7. Example of the line-shape analysis of the 1128 keV $10^+ \rightarrow 8^+$ transition in ^{82}Zr. The observed and fitted (thick lines) line-shapes in the backward ($\overline{\Theta} = 145°$) and the forward ($\overline{\Theta} = 35°$) Ge-detector rings are shown in (a) and (b). (c) illustrates the distribution of fit results to the line shapes in (a) and (b) using the feeding pattern shown in (d) and a Monte Carlo variation of the feeding times within their errors. The vertical line in (c) represents the peak position of a Gaussian fit to this distribution, the dashed lines correspond to the FWHM of that fit. In Table VI a 20% systematic error is added due to uncertainties in the stopping-power function and sidefeeding times.

$[R_{\mathrm{DCO}} = 0.47(7)]$ was used to fix the spin and parity of the 2857 keV level. Thereafter, the DCO ratios of the $\Delta I = 1$, 271, and 378 keV as well as higher lying $E2$ transitions were used to determine the spins within that band. A number of single and doubly gated spectra indicated an enhanced intensity for the 1072 keV $16^- \rightarrow 14^-$ transition suggesting the tentative structure in the lower right corner of Fig. 5.

Due to the comparatively clean gating conditions mentioned above, it was possible to deduce a few lifetimes for states in the yrast $(+,0)$ band from the backed target experiment. The results are summarized in Table VI, including the lifetime values deduced earlier for the two lowest states [46]. An example of a Doppler-shifted line-shape analysis is presented in Fig. 7. The line shape of the 1128 keV $10^+ \rightarrow 8^+$ transition is shown at backward [$\overline{\Theta} = 145°$, Fig. 7(a)] and forward [$\overline{\Theta} = 35°$, Fig. 7(b)] angles. The thick lines represent the results of least-squares fits to the spectra. Based on the stopping-power theory of Lindhard *et al.* [47] the velocity distribution of the recoiling nuclei was Monte Carlo simulated with the code DESASTOP [48,49]. The Q value of the reaction and the energy and angular distributions of the evaporated light particles, the angular straggling of the recoils, and the opening cone of the Ge detectors were taken into account.

The lifetime of the 6491 keV 14^+ state was determined effectively; i.e., without corrections for the side and cascade feeding, as the lifetimes of higher lying discrete levels are unknown. For the determination of the lifetimes of the lower lying states, both side and cascade feeding was included. The peak of the 847 keV $6^+ \rightarrow 4^+$ transition showed no obvious Doppler-broadened line shape. Hence, a lifetime for the 1888 keV 6^+ state could not be deduced. Figure 7(d) illustrates the feeding pattern used for the 1128 keV $10^+ \rightarrow 8^+$ transition. The sidefeeding times were taken from an empirically parametrized correlation between the excitation energy E_x and the sidefeeding time τ_{sf} in this mass region presented in Ref. [50]. A generous uncertainty of 30% was imposed on these feeding times since they may vary considerably from nucleus to nucleus or even from rotational band to rotational band [51]. To account for the uncertainties in the side- and cascade-feeding pattern, least-squares fits were performed with the feeding times and intensities varied randomly within their errors. Figure 7(c) shows the distribution of the fitted lifetimes of the 4037 keV 10^+ level for 500 different feeding scenarios. In Table VI the centroid of this distribution is adopted as the lifetime. The error corresponds to the full width at half maxima of distributions such as Fig. 7(c). An additional 20% systematic error accounts for possible uncertainties in the slowing-down process.

III. DISCUSSION

The high-spin data of the $T_z = 1$ Kr, Rb, Sr, and Zr nuclei have been analyzed using the pairing-and-deformation self-consistent total Routhian surface (TRS) model. The model is based on the macroscopic-microscopic method of Strutinsky [52]. The macroscopic part of the total energy is calculated according to the mass formula of Ref. [53] and the single-particle potential is of Woods-Saxon type. The pairing channel includes seniority and doubly stretched quadrupole pairing interactions to avoid spurious shape dependence [54]. To avoid a superfluid-to-normal phase transition due to the mean-field approximation, we employ an approximate particle-number projection known as the Lipkin-Nogami method [55,56]. The total Routhian (expectation value of the cranking Hamiltonian in the rotating frame of reference) is minimized with respect to the quadrupole (β_2, γ) and hexadecapole (β_4) deformation parameters. The details of our calculations strictly follow Refs. [56,57]. The present version of our code allows us to block self-consistently only the lowest quasiparticle states in each parity-signature (π, α) block. In the following we will use the standard spectroscopic notation, namely A, B, E, and F, to label the 1qp configurations that correspond to $(+,+)$, $(+,-)$, $(-,-)$, and $(-,+)$ combinations of parity and signature quantum numbers, respectively.

The low level density of nuclear states simplifies possible theoretical assignments of the low lying excited bands in terms of 2qp excitations. The single-particle orbitals of interest are [431]3/2 and [312]3/2 (and to some extent [310]1/2 and [303]7/2) below the $N = 38$ subshell closure, the [422]5/2 orbital separating the $N = 38$ and $N = 40$ subshell gaps, and the [301]3/2 and (at even larger deformation) [431]1/2 states above the $N = 40$ shell gap. The appropriate Nilsson diagrams are presented in Fig. 8. In our calculations, only the [431]3/2 orbital shows large signature splitting at large prolate deformation. At this shape some signature splitting is also predicted for the [310]1/2 orbital but the remaining states listed above do not show any sizable signature splitting. The calculated signature splittings of the [431]3/2, [422]5/2, [312]3/2, and [301]3/2 orbitals agree well with the empirical data in, e.g., the odd-A nuclei ^{75}Rb, ^{77}Rb, ^{77}Sr, and ^{79}Sr (see, e.g., [58]). One might expect signature splitting to be present in the [431]1/2 orbital. However, in terms of the spherical shell model the [431]1/2 state is a mixture of orbitals originating from the $d_{5/2}$ and $g_{7/2}$ states that have

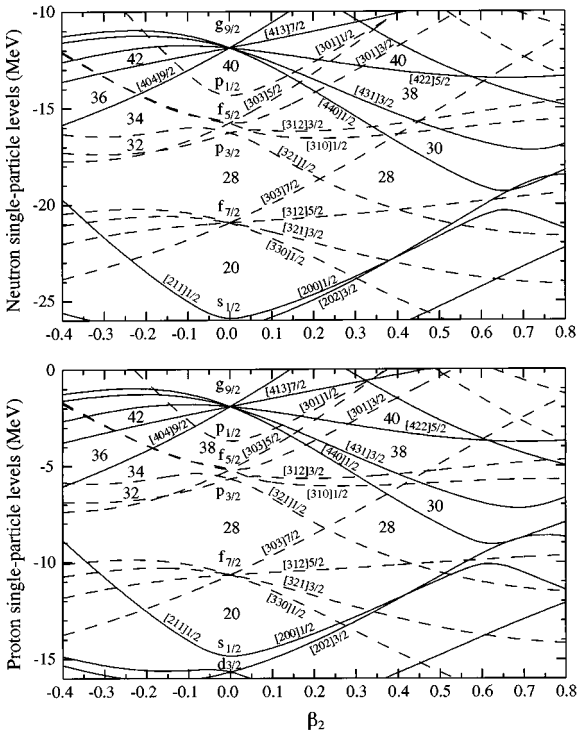

FIG. 8. Neutron (top) and proton (bottom) single-particle levels in ^{78}Sr as a function of the quadrupole deformation $\beta_2(\beta_4=0)$ deduced from a Woods-Saxon potential. The diagrams are representative for $N\approx Z$ nuclei in the $A\approx 80$ mass region. Positive-parity orbits are indicated with solid lines, negative-parity orbits with dashed lines. The spherical quantum numbers are given as well as the asymptotic Nilsson quantum numbers $[Nn_z\Lambda]\Omega$. Note that especially some of the negative-parity levels are strongly mixed. The numbers denote the nucleon numbers at pronounced or important shell gaps.

opposite signature splitting. The resulting lack of signature splitting is, therefore, due to cancellation that appears at large prolate deformations only.

The calculated minima at large deformations are predicted to be rather shallow and to coexist with oblate structures. The shallowness of the energy surface is indicated by, e.g., the low lying γ-vibrational bands that are commonly observed experimentally in this region. The 2_2^+ states lie at an excitation energy of 1.204 MeV in ^{74}Kr, possibly at 1.478 MeV in ^{78}Sr, and at 1.061 MeV in ^{82}Zr. The vibrational degrees of freedom are beyond our model and neither the γ-vibrational bands nor vibration-rotation coupling are included in the discussion in a quantitative way. The shape softness further implies (at least theoretically) that the shape is very sensitive to the rotation-induced alignments. In fact, almost all the calculated bands in this mass region show pronounced shape changes at rotational frequencies corresponding to the alignments of nucleons occupying states originating from $\pi g_{9/2}$ and $\nu g_{9/2}$ subshells. Satisfactory agreement between theory and experiment in the $T_z=1$ nuclei analyzed here as well as in the $T_z=1/2$, ^{75}Rb and ^{77}Sr nuclei analyzed in Ref. [58] supports this scenario. Recently, the lifetimes in positive-parity bands of ^{77}Rb have been measured and the extracted transitional quadrupole moments decrease substantially as a function of rotational frequency [26] which strongly supports the scenario of a shape change.

A. Band structures in ^{74}Kr

1. The positive-parity bands

The irregular pattern at the beginning of the positive-parity yrast band in ^{74}Kr ($Z=36$, $N=38$) is attributed to a prolate-oblate shape mixing at low spins [5,7]. Thereafter, a well-deformed prolate band evolves and the irregularity around spin $I=14$ has been interpreted as due to the simultaneous alignments of the proton and neutron $g_{9/2}$ orbitals [21].

The calculated and experimental Routhians for positive- and negative-parity bands in ^{74}Kr are shown in Figs. 9(a) and 9(b). Due to the $N=38$ subshell closure, neutron 2qp excitations are predicted to lie at much higher excitation energies than the 2qp proton excitations over the entire frequency range. The lowest 2qp positive-parity band is, therefore, expected to be built on a $(\pi g_{9/2})^2$ (AB) configuration. The 2qp positive-parity band involving negative-parity orbitals like $\pi[312]3/2$ (the EF configuration) is predicted to lie higher in energy, at least at low spins. These observations are in agreement with the exprimental Routhians of ^{75}Rb [58].

The agreement between theory and experiment for the positive-parity bands is satisfactory [see Fig. 9(a)]. The crossing between ground-state band (gsb) and S band at $\hbar\omega\approx 0.65$ MeV is well accounted for in the calculations, as illustrated in Fig. 9(b). Its structure is rather complex: The alignment of a pair of $g_{9/2}$ protons induces a shape change resulting in a simultanous alignment of $g_{9/2}$ neutrons that in turn induces even larger shape distortions, as suggested and discussed in detail in Ref. [21]. In particular, the quadrupole deformation of this band is predicted to drop from $\beta_2\approx 0.38$ at low frequencies to below $\beta_2\approx 0.30$ after the alignment. This is accompanied by a substantial change in the hexadecapole deformation from $\beta_4\approx 0.0$ to almost $\beta_4\approx -0.05$, but the shape is predicted to remain prolate. The magnitude of these changes is typical of most of the bands calculated here but, with increasing mass, the aligning $g_{9/2}$ quasiparticles lead to triaxial shapes.

The excited band reveals a clear shift of the crossing frequency with respect to the gsb by $\Delta(\hbar\omega)\approx 0.3$ MeV [see Fig. 9(a)]. This shift is a natural result of the blocking of the $\pi[431]3/2$ orbital. The observed band crossing is due to the alignment of a $(\nu g_{9/2})^2$ neutron pair. At large prolate deformation, the neutron $(\nu g_{9/2})^2$ alignment is expected to take place at larger rotational frequencies than the corresponding proton $(\pi g_{9/2})^2$ alignment due to the position of the neutron Fermi level which is higher in the $g_{9/2}$ shell. The shift of the crossing frequency supports the $(\pi g_{9/2})^2$ assignment for the observed 2qp band. However, at low frequencies, our model clearly underestimates the excitation energy of this band. Moreover, relatively strong linking transitions to the gsb make it difficult to pursue a pure 2qp scenario, suggesting possibly vibrational admixtures.

2. The negative-parity bands

At prolate deformation, the negative-parity bandheads can be easily generated by breaking a pair of protons below the $N,Z=38$ gap rather than exciting a neutron across the gap. Possible configurations are $\pi[312]3/2\otimes\pi[431]3/2$, and, energetically less favored, $\pi[310]1/2\otimes\pi[431]3/2$, or $\pi[303]7/2\otimes\pi[431]3/2$. The calculation assigns the two

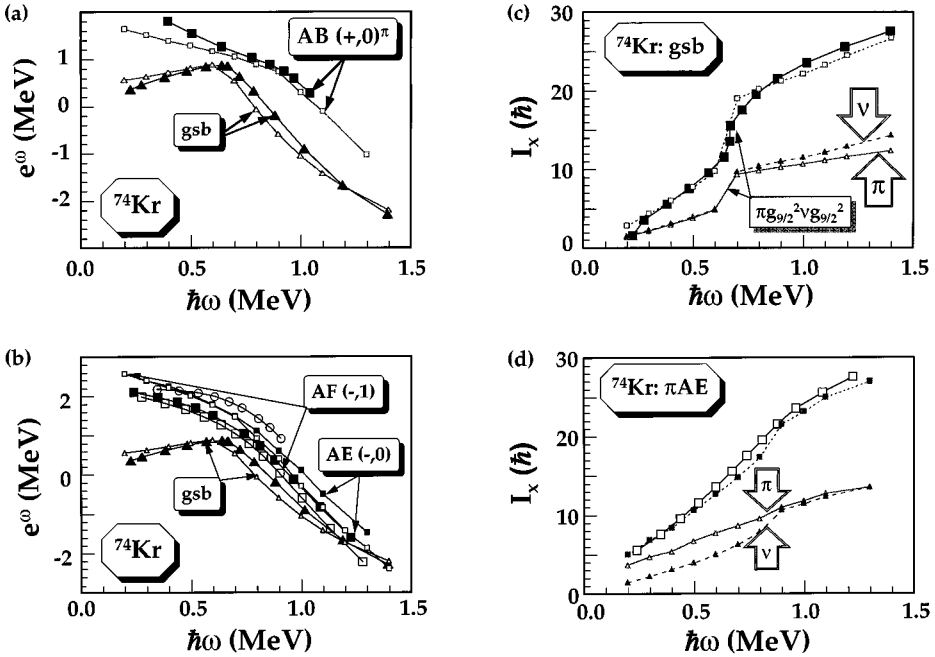

FIG. 9. Theoretical and experimental cranked-shell model quantities for ^{74}Kr. (a) The experimental (solid symbols) and theoretical (open symbols) Routhians vs the rotational frequency for the positive-parity ground-state band (gsb) and the signature $\alpha=0$ sideband (AB). (b) The experimental (large symbols) and theoretical (small symbols) Routhians vs the rotational frequency for the negative-parity side bands in ^{74}Kr. Open (solid) squares denote configurations of signature $\alpha=-1$ (0), respectively. Open circles denote the empirical data for the weakest negative-parity sideband. The triangles label the results for the gsb. These data are included here to illustrate the relative excitation energy scheme as a function of rotational frequency. (c) The aligned angular momentum vs rotational frequency for the gsb in ^{74}Kr. Large symbols denote the empirical data while small symbols label the result of the calculations. The individual proton and neutron contributions to the I_x are depicted separately. (d) A plot of the aligned angular momentum as a function of rotational frequency for the negative-parity sideband of signature $\alpha=0$ (AE) in ^{74}Kr. Open squares denote the empirical data while solid squares denote the result of the calculations. The individual proton and neutron contributions are also shown. The agreement between the data and the calculations for the $\alpha=1$ signature partner (AF) is similar.

lowest, strongly populated, negative-parity bands as $\pi\,[431]_{\alpha=1/2}\otimes\pi\,[312]_{\alpha=\pm1/2}$. The calculated bands nicely reproduce the experimental data but show an offset of the order of $\approx$300 keV in excitation energy relative to the gsb. A similar shift is obtained for the $[312]3/2_{\alpha=\pm1/2}$, 1qp bands in ^{75}Rb [58] suggesting that the relative position of the $g_{9/2}$ and $f_{5/2}$ orbitals is misplaced by the corresponding amount in our Woods-Saxon potential. Small deviations for the calculated signature splitting are also seen but, as discussed in Ref. [58], the signature splitting of the $[312]3/2$ orbital is very sensitive to the triaxiality of the shape and can easily be inverted when γ changes sign.

The third (weakest) negative-parity band can be assigned as the $\pi\,[431]_{\alpha=1/2}$ coupled to the $\pi[310]1/2$ (pseudospin partner of $[312]3/2$) or the $\pi[303]7/2$ orbital. Since the rotational bands build upon the high-K $[303]7/2$ orbital are strongly coupled, one expects to experimentally observe both signature partners. Observation of only one branch favors the $\pi[310]1/2$ orbital. The signature splitting of this orbital depends strongly on triaxiality and the observation of the $\alpha=1$ branch speaks in favor of a negative γ value.

Interestingly, the Routhians of the $[312]3/2$ orbit behave quite similarly to the $[301]3/2$ orbit — essentially flat with increasing frequency. The latter was interpreted as a ''spectator'' orbital which possibly gives rise to the ''identical'' bands observed in ^{77,78}Sr and ^{78}Rb [34]. By subtracting (adding) a proton from (to) the configuration $\pi[312]3/2\otimes\pi[431]3/2\otimes(\nu[431]3/2)^2$, the positive-parity sequence in ^{73}Br [59] (^{75}Rb [58]) can be reached. In Fig. 10 the dynamic moments of inertia and the alignments i of these bands are compared. Even though they are not ''identical'' [60] they behave very similarly, especially in the case of the negative-parity bands in ^{74}Kr and the positive-parity band in ^{75}Rb. The range of interaction between the ground-state and aligned 2qp neutron bands is exceptionally broad ($\Delta\hbar\omega\approx0.5$ MeV). This may not be fully explained by the large $N=38$ shell gap [61,58]. The additional presence of strong residual $T=0$ n-p pairing in the course of the alignment in these bands might smooth the alignment pattern. After the $N=38$ $g_{9/2}$ alignment a single proton and a single neutron are left in exactly the same $[431]3/2$ Nilsson orbit for the positive parity in ^{75}Rb and the negative parity in ^{74}Kr. However, there is not an obviously large discrepancy between the experiment and the standard calculations (neglecting n-p pairing correlations) in either ^{75}Rb [58] or ^{74}Kr [see also Fig. 9(d)] that would definitely call for invoking collective $T=0$ pairing.

B. The odd-odd $T_z=1$ nucleus ^{76}Rb

To obtain a better perspective on how well our theoretical calculations are able to reproduce the known properties of the $T_z=1$ nuclei, we include here a discussion of the odd-odd nucleus ^{76}Rb studied in Ref. [35].

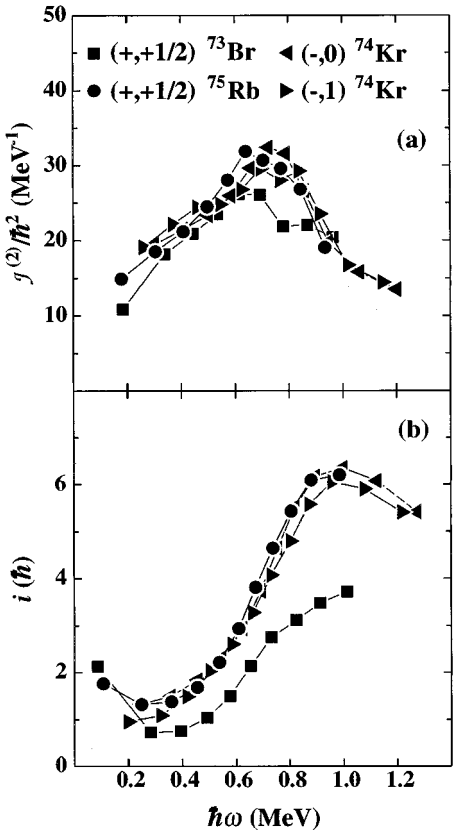

FIG. 10. Dynamic moments of inertia $\mathcal{J}^{(2)}$ and alignments i of rotational bands in ^{74}Kr ($\pi=-,\alpha=0,1$), ^{73}Br (+,+1/2), and ^{75}Rb (+,+1/2). They are considered to be ''identical'' with respect to the presence or absence of protons in the [312]3/2 orbital in their intrinsic configuration.

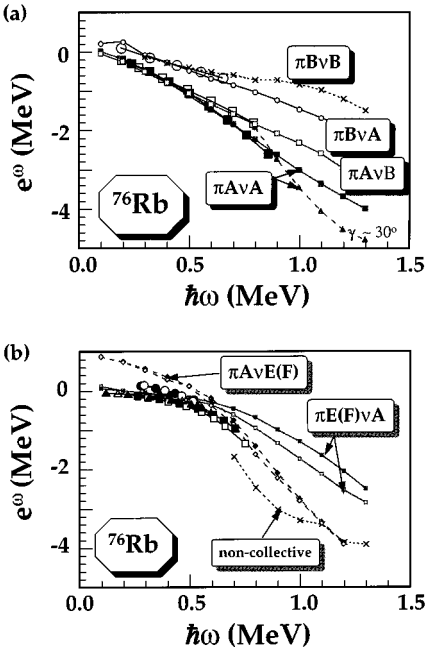

FIG. 11. Theoretical and experimental cranked-shell model quantities for ^{76}Rb. (a) The experimental (large symbols) and theoretical (small symbols) Routhians vs the rotational frequency for the positive-parity bands. The empirically observed bands are interpreted as the three most favored signature combinations of the $\pi[431]\otimes\nu[422]$ quadruplet, namely the πAνA, πAνB and πB νA configurations. The very unfavored signature member of this quadruplet, the $\pi B\nu B$ configuration is also shown as well as the triaxial ($\gamma\approx-30°$) structure. See text for further details. (b) The experimental (large symbols) and theoretical (small symbols) Routhians vs rotational frequency for the negative-parity bands. Only two signature combinations (EA and FA) of the $\pi[312]\otimes\nu[422]$ quadruplet are shown for the reason of clarity. The open and solid diamonds indicate negative-parity bands built upon the $\pi[431]\otimes\nu[301]$ configuration. The yrast noncollective structures are also shown.

The energetically most favored rotational bands in this nucleus are calculated to involve the $\nu[422]5/2$ orbital coupled to a state from below the $Z=38$ subshell closure. The positive-parity bands, therefore, are expected to form a quadruplet of bands involving the various possible signature combinations of the $\pi[431]3/2\otimes\nu[422]5/2$ orbits. The large signature splitting of the $\pi[431]3/2$ counteracts the small signature splitting of the $\nu[422]5/2$ orbital. With increasing rotational frequency, an average signature splitting develops due to the Coriolis mixing (see also ^{77}Sr [34]). The quadruplet of positive-parity bands will split into two doublets. Namely, the so-called AA and AB configurations involving $\pi[431]_{\alpha=1/2}\otimes\nu[422]_{\alpha=\pm1/2}$ will lie lower than the so-called BA and BB bands built on $\pi[431]_{\alpha=-1/2}\otimes\nu[422]_{\alpha=\pm1/2}$ configurations, respectively. Note, that (i) both available high-j orbitals are blocked and (ii) static pairing correlations are rather weak because of blocking. One might even consider these configurations as effective doubly magic structures. Therefore, the theoretical Routhians are expected to be almost unperturbed by nuclear rotation over a wide frequency range. All these simple considerations are well accounted for by the calculations as is shown in Fig. 11(a). Our results are in excellent agreement with the experimental data [35] implying that the signature splitting properties of the orbitals originating from the $g_{9/2}$ subshell are properly taken into account (see again ^{77}Sr as discussed in [58]).

At low rotational frequencies, the well-deformed negative-parity structures involve the ν [422]5/2 orbital coupled to the negative-parity states from below the $Z=38$ gap. The lowest configuration is expected to involve all possible signature combinations of [422]5/2$\otimes$[312]3/2 and, at low rotational frequencies, would form a quadruplet of almost degenerate bands as observed experimentally. For reasons of clarity, only two out of four ν [422]5/2$\otimes\pi$ [312]3/2 configurations are shown in Fig. 11(b). The remaining two combinations are degenerate at low spins with the ones presented in the figure. The excitation energy is fairly well reproduced but the theory predicts for these configurations rather small deformation changes at the crossing frequency and, therefore, the yrast-yrare interactions are strongly overestimated. The π [431]$\otimes\nu$ [301] configuration is predicted to lie higher in excitation energy at low frequencies but it aligns more angular momentum because of a smaller deformation and becomes strongly favored in energy above $\hbar\omega\approx0.6$ MeV. Note also low lying, noncollective configurations at frequencies above $\hbar\omega\approx0.6$ MeV. Two additional negative-parity bands observed in this nucleus can be interpreted as either $\nu[422]\otimes\pi[310]$ or $\nu[422]\otimes\pi[303]$. The observed small signature splitting would favor the latter as-

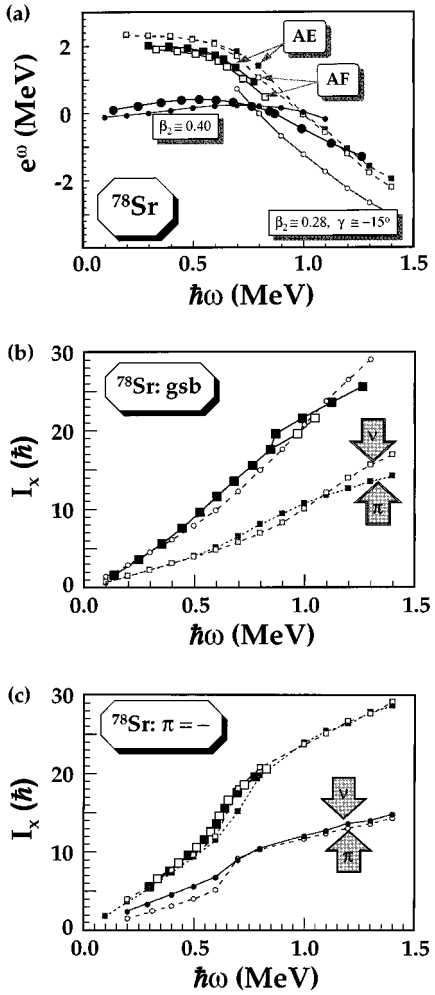

FIG. 12. (a) The experimental (large symbols) and theoretical (small symbols) Routhians vs the rotational frequency for the ground-state band and negative-parity sidebands in ^{78}Sr. At $\hbar\omega > 0.8$ MeV our calculations strongly favor energetically the triaxial ($\gamma \approx -15°$) structure marked by open circles. See text for further details. (b) The aligned angular momentum vs the rotational frequency for the gsb. The empirical data are marked with large symbols while small symbols indicate the theoretical results. (c) The aligned angular momentum vs the rotational frequency for the negative-parity sidebands in ^{78}Sr. The empirical data are marked with large symbols while small symbols again indicate the theoretical results.

signment. The assignments agree well with the previous suggestions in Ref. [35].

C. Band structures in ^{78}Sr

1. The positive-parity bands

The $Z=38$ and $N=40$ proton and neutron subshell closures stabilize the shape of the nucleus. The calculated gsb is predicted to be well deformed ($\beta_2 \approx 0.4$) and stable over a large frequency range. At this shape both proton and neutron alignments are predicted to be very smooth [large interaction, see Fig. 12(a)]. Experimentally, the interaction is even stronger and the experimental and theoretical I_x curves show different trends. Moreover, the data clearly indicate (i) the existence of an energetically favored 14^+ state while in the

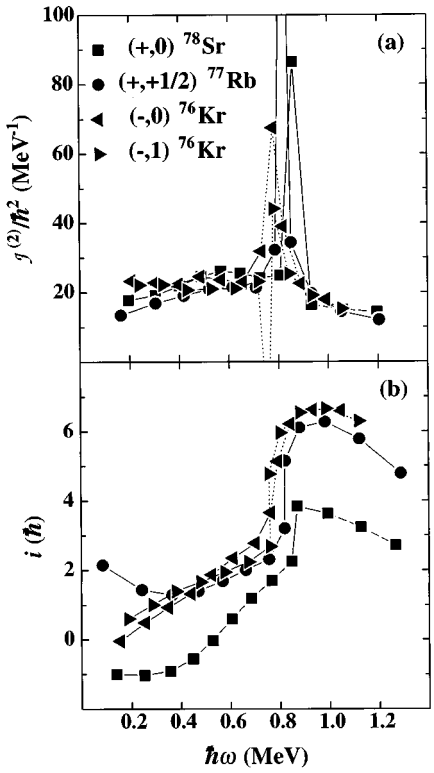

FIG. 13. Dynamic moments of inertia $\mathcal{J}^{(2)}$ and alignments i of the ^{76}Kr $(-,0)$, ^{77}Rb $(+,+1/2)$, and ^{78}Sr $(+,0)$ *yrast* cascades. The band crossing in ^{77}Rb was attributed to a change in the occupation of the orbits near the neutron Fermi level of the valence *pair* of neutrons [26].

calculations, the 16^+, $\pi g_{9/2}^2 \otimes \nu g_{9/2}^2$, configuration is predicted to be favored and (ii) the yrast band forks above spin 18^+ which is difficult to explain within the TRS model. Our calculations indicate the existence of low lying triaxial structures which are becoming yrast at the rotational frequency corresponding to the frequency where the forking takes place. However, the calculated values of the aligned angular momentum, $I_x = \langle \hat{j}_x \rangle$, exceed the experimental values by ~ 3 for this configuration. In fact, our calculations predict the triaxial configurations to become more and more favored with $Z > 38$ and $N > 38$. The theoretical check of the suggestion that the left branch of the forking (see Fig. 3) can be attributed to a so-called ''unpaired'' band crossing (see below) would require a full diabatic tracing of the configurations near the neutron Fermi level. This has been done in Ref. [26] but would exceed the frame of the current investigation.

Recently, a so-called ''unpaired'' band crossing [62] has been reported for the nucleus ^{77}Rb [26]. Two positive-parity rotational bands of the same signature were observed over a wide range of frequencies ($I = 9/2$–$45/2$). They change the yrast character at $\hbar\omega \approx 0.8$ MeV but since the yrare band also starts at low spins the conventional band-crossing mechanism of two aligning high-j neutron quasiparticles is excluded. In fact, the moments of inertia and the measured transition quadrupole moments indicate that a strongly deformed band ($\beta_2 \approx 0.4$) is crossed by a less deformed band ($\beta_2 \approx 0.3$). A diabatic tracing of the configurations near the neutron Fermi energy attributes this crossing to a change in

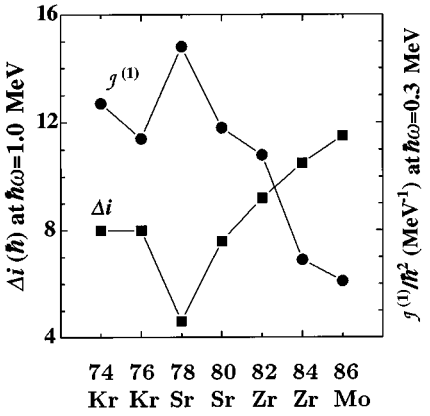

FIG. 14. Kinematic moments of inertia $\mathcal{J}^{(1)}$ at a rotational frequency of $\hbar\omega=0.3$ MeV for the positive-parity yrast bands in a series of even-even $T_z=1$ and $T_z=2$ nuclei in the vicinity of ^{78}Sr (solid circles). The alignment Δi at $\hbar\omega=1.0$ MeV of these bands relative to the Harris parametrization [64] $(\mathcal{J}_0,\mathcal{J}_1,i_0)=(18,0,0)$ is also shown (solid squares). In the case of ^{78}Sr the yrare branch above the forking (see Fig. 3) was used for reasons discussed in the text.

the orbitals occupied by the valence neutron *pair* — the $\pi[431]3/2\otimes(\nu[422]5/2)^2$ configuration is favored at low frequencies, the $\pi[431]3/2\otimes(\nu[301]3/2)^2$ configuration at high frequencies. This feature should be unique to (i) the particle number $N,Z=40$ (see Fig. 8, Ref. [26]) with (ii) the first $g_{9/2}$ alignment of the other kind of nucleons suppressed. Therefore, other good candidates are the negative-parity bands in ^{76}Kr, the positive-parity bands in ^{78}Sr and ^{80}Zr, and the negative-parity bands in ^{81}Zr. The latter two are yet to be identified (at high spins). Hence, the $\mathcal{J}^{(2)}$ moments of inertia and the alignments i of the ^{76}Kr $(-,0)$, ^{77}Rb $(+,+1/2)$, and ^{78}Sr $(+,0)$ *yrast* cascades (to highlight the so-called ''unpaired'' crossing) are shown in Fig. 13. Indeed, the bands in ^{76}Kr and ^{78}Sr also provide a crossing at high rotational frequencies, and the standard type Woods-Saxon calculations (see above) cannot reproduce the crossing at least in ^{78}Sr. However, in contrast to ^{77}Rb, only a forking is observed in the even-even isotones, not two sequences persisting from very low to very high spins. Clearly, more detailed spectroscpic data are necessary, and future detailed configuration-dependent cranking calculations including pairing (which are beyond the scope of the present paper) may provide insight into this phenomenon.

Clearly, the two large gaps at $N,Z=38,40$ at a prolate deformation of $\beta_2\approx0.4$ (see Fig. 8) are dominating the nuclear structure of the nuclei in the vicinity of ^{78}Sr. However, for $N,Z=36$ or $N,Z\geq42$ the energy gaps on the oblate side are expected to be competitive. Large shell gaps lead to a reduction of the pairing strength which may result in near rigid rotation already at low rotational frequencies. Near rigid rotation is generally presumed if the kinematic moment of inertia $\mathcal{J}^{(1)}$ equals the dynamic moment of inertia $\mathcal{J}^{(2)}$ over a wide frequency range although the sum of the microscopic contributions to the moments of inertia may ''accidentally'' satisfy this condition. Here, the most prominent example of rigid rotation is the positive-parity yrast band in ^{77}Rb ($Z=37$, $N=40$). The subject was extensively discussed by Lühmann *et al.* [16] and recently shown to persist to even higher spins [26]. Similarly, the energetically favored negative-parity bands in ^{76}Kr ($Z=36$, $N=40$) provide $\mathcal{J}^{(1)}\approx\mathcal{J}^{(2)}$ [15,63] as well as several bands in the odd-odd system ^{76}Rb [35]. Figure 14 shows the kinematic moments of inertia for the positive-parity yrast bands of a series of even-even $T_z=1$ and $T_z=2$ nuclei (solid circles) at the rotational frequency of $\hbar\omega=0.3$ MeV. This typically corresponds to $I\approx4$. The distinct spike in the $\mathcal{J}^{(1)}$ of ^{78}Sr adds further evidence for the predicted large shell gaps and, hence, to the assumption that these nuclei have such large prolate ground-state deformations. As compared to ^{78}Sr the moments of inertia $\mathcal{J}^{(1)}$ for the self-conjugate nucleus ^{76}Sr (^{80}Zr) are slightly larger (smaller). If (i) small changes in the pairing and (ii) possible small variations in the low-spin configuration mixing are negligible, the gap at $N,Z=38$ should be somewhat larger than the one at $N,Z=40$ which is in agreement with the predictions. The reduced pairing strength shall lead to flatter Routhians because the $N,Z=38$ gap persists to very high frequencies ($\hbar\omega>1$ MeV) [2]. As a consequence, smaller alignments along the rotational bands are expected. The alignments Δi at $\hbar\omega=1.0$ MeV are included in Fig. 14 as the solid squares. They were calculated relative to a reference rotor according to the Harris parametrization [64] $(\mathcal{J}_0,\mathcal{J}_1,i_0)=(18,0,0)$. For ^{78}Sr the yrare branch above the forking (see Fig. 3) was used (see Sec. II B, the yrast branch would add only one additional unit). The ''symmetric'' course of the moments of inertia and the alignments in Fig. 14 fit well into the scenario described above.

2. The negative-parity bands

The sidebands appear to follow the scenario of simple 2qp excitations and they are assigned as $\nu[422]\otimes\nu[301]$ configurations. Due to the closed prolate-deformed $Z=38$ and $N=40$ shells, the negative-parity bands are high in excitation energy and only weakly populated. This might be the main reason why they have not been observed in previous investigations. As the $N=40$ gap seems to be only slightly smaller than the $Z=38$ gap (see above) one expects to identify negative-parity bands built upon neutron as well as proton 2qp states at similar excitation energies. The possible configurations are (i) $\pi^2[431]3/2\otimes\nu[422]5/2\otimes\nu[301]3/2$ $(K=4)$; (ii) $\pi[431]3/2\otimes\pi[301]3/2\otimes(\nu[422]5/2)^2$ $(K=3)$; or (iii) $\pi[312]3/2\otimes\pi[422]5/2\otimes(\nu[422]5/2)^2$ $(K=4)$, respectively.

Based on systematics, the (neutron-excited) configuration (i) can be assigned to the more strongly populated signature-partner bands in the middle of Fig. 3: By removing or adding a neutron in the presumed [301]3/2 ''spectator'' orbital the positive-parity yrast bands in ^{77,79}Sr can be reached. Consequently, the dynamic moments of inertia, experimental Routhians e', and alignments i of these bands are illustrated in Fig. 15. All bands exhibit a common (proton) band crossing at $\hbar\omega\approx0.6$ MeV underlining their similar structure. The gain in alignment $(\Delta i\approx5)$ is typical for an aligned pair of $g_{9/2}$ nucleons. The cranked-shell model quantities for the second negative-parity band seem to behave similarly to the positive-parity yrast cascade in ^{77}Rb $[\pi[431]3/2\otimes(\nu[422]5/2)^2]$. The tentative 3^- state at 2310 keV excitation energy also speaks in favor of the proton-excited con-

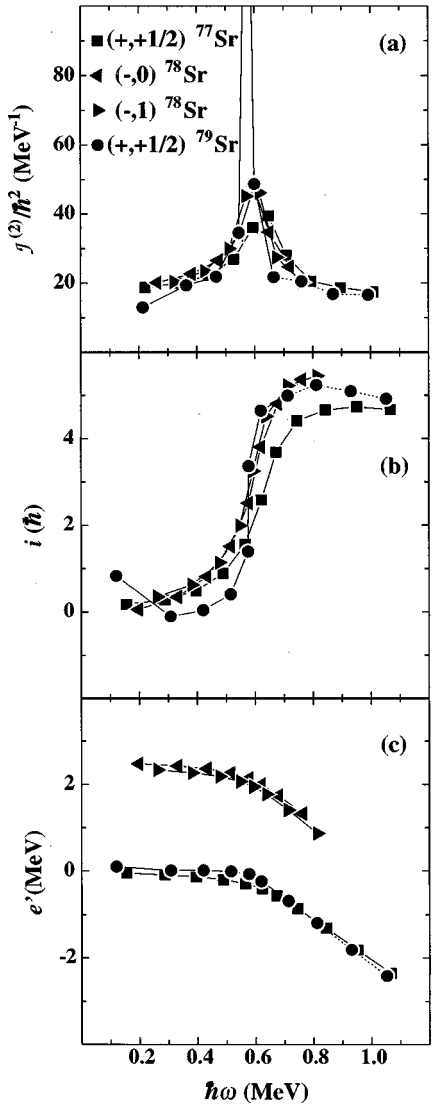

FIG. 15. Dynamic moments of inertia $\mathcal{J}^{(2)}$, experimental Routhians e', and alignments i of rotational bands in ^{78}Sr ($\pi=-,\alpha=0,1$), and ^{77,79}Sr $(+,+1/2)$. They are considered to be ''identical'' with respect to the presence or absence of neutrons in the [301]3/2 orbital in their intrinsic configuration.

figuration (ii) mentioned above. However, lack of experimental data in ^{78}Sr itself and ^{79}Y, i.e., one proton added to the configuration (iii), does not allow for a definite assignment.

In the calculations, the excitation energy of these bands is overestimated by a constant value of $\Delta e^{\omega}\approx 400$ keV over the entire frequency range [see Fig. 12(a)]. We believe that this shift is rather due to an inaccurate treatment of the gsb, where the coupling to the vibrational degrees of freedom is not taken into account. The calculated and experimental values of the angular momentum agree very well as shown in Fig. 12(b). This and the result obtained for ^{74}Kr (see discussion above) support the conclusion steming from the RPA calculations of Ref. [65] that the negative-parity sidebands in these nuclei are almost pure 2qp excitations.

D. Triaxial rotation in the $Z>38$ nuclei

In contrast to ^{74}Kr and ^{78}Sr, the number of protons in ^{82}Zr exceeds $Z=38$. Similarly, its neutron Fermi level falls

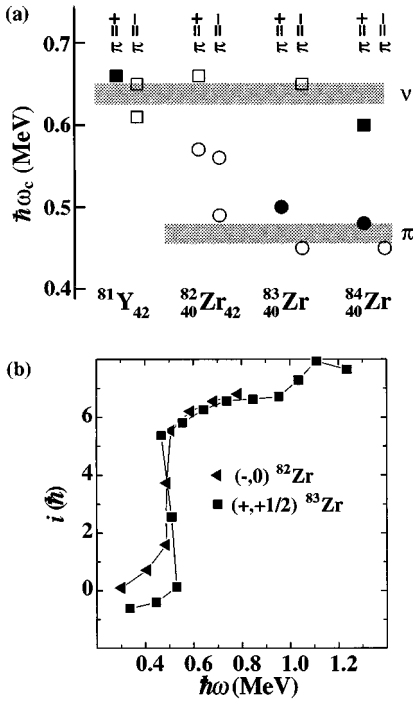

FIG. 16. The upper part shows band-crossing frequencies of pairs of $g_{9/2}$ nucleons for ^{82}Zr and neighboring nuclei. Squares denote known (solid) and assigned (open) neutron crossings, circles denote proton crossings. In the lower part the alignments i of rotational bands in ^{82}Zr ($\pi=-,\alpha=0$) and ^{83}Zr $(+,+1/2)$ are shown.

beyond the gaps at $N=38$ and 40 which drive the lighter nuclei towards large prolate deformation. In fact, the measured lifetimes indicate a deformation of $|\beta_2|\approx 0.3$ rather than 0.4 for the positive-parity yrast cascade in ^{82}Zr. This band is predicted to start at a prolate-deformed shape (see, e.g., Refs. [2,45]) and its evolution is interpreted as a proton $g_{9/2}$ crossing followed by a neutron $g_{9/2}$ crossing [45]. Though the second band crossing is now found to occur at $\hbar\omega\approx 0.65$ MeV (as compared to $\hbar\omega\approx 0.69$ MeV in Ref. [45]) the arguments presented in Ref. [45] are still valid. The upper part of Fig. 16 shows the band-crossing frequencies $\hbar\omega_c$ of ^{82}Zr and some of its neighbors. The squares represent the known (solid symbol) or suggested (open symbol) neutron alignments and the circles are proton alignments. In the $(+,+1/2)$ band in ^{81}Y [66,67] the first proton alignment is blocked. Hence, the crossing at $\hbar\omega\approx 0.67$ MeV is attributed to a neutron crossing. According to lifetime measurements this crossing is supposed to induce a shape change from a well-deformed prolate shape ($\beta_2\approx 0.35$) towards a triaxial ($\gamma\approx -30°$) configuration [68]. In the $(+,+1/2)$ band in ^{83}Zr [69,70] the first neutron alignment is blocked. By means of the measured sign of the mixing ratio $\delta(E2/M1)$ of a low lying transition the band was found to be (nearly) oblate [$\beta_2=-0.28(2)$] and built upon the $[422]5/2^+$ Nilsson orbital [69]. The shapes of the negative-parity bands, however, are prolate. Mountford *et al.* [71] demonstrated with a g-factor measurement that the aligning particles responsible for the first crossing in ^{84}Zr are protons. In the ground state and at low rotational frequencies calculations indicate a triaxial shape ($\beta_2\approx 0.28$, $\gamma\approx -20°$) for this nucleus, and the crossing frequencies are well reproduced [72,73]. The ''de-

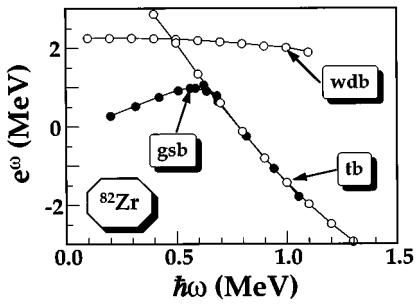

FIG. 17. The curve marked by solid dots represents the experimental Routhian of the gsb in ^{82}Zr. Theoretical calculations are marked with open circles and the curve marked as ''wdb'' corresponds to the well-deformed band which is calculated to be yrast at low rotational frequencies. ''tb'' denotes the triaxial band which is yrast at high spins. Its exciation energy was normalized to the experimental data. The figure clearly illustrates the difficulties in reproducing the data for $Z>38$ and $N>38$ nuclei.

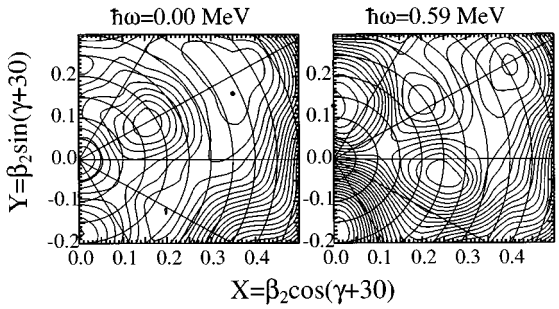

FIG. 18. The total Routhian surface calculated at low rotational frequency (left panel) and high rotational frequency (right panel) in ^{82}Zr. The distance between the contour lines amounts to 200 keV. Note an extreme quadrupole shape softness at low spins which is found to be the primary source of disagreement between the model (purely rotational) and the data in ^{82}Zr.

layed'' proton crossing in the positive-parity band of ^{82}Zr (see Fig. 16) adds evidence for a well-deformed prolate ground state. The crossing frequencies of the aligning protons of the prolate-deformed bands of the somewhat lighter isotopes (see, e.g., Fig. 15) amount to $\hbar\omega\approx 0.6$ MeV. Generally, it seems that nuclei beyond the shell gaps at $N,Z=38,40$ are again susceptiple to shape coexistence; i.e., the $N=42$ shell gap at oblate deformation might play a significant role (see Fig. 8).

Shape coexistence might also occur in the negative-parity bands of ^{82}Zr. A 2qp proton excitation generating the negative parity is unlikely due to the gap in the single-particle energies (see Fig. 8). At prolate deformation, a possibly proton-excited bandhead configuration is $\pi[422]5/2 \otimes \pi[301]3/2$. However, if one of the two negative-parity bands of ^{82}Zr were built upon this state it should behave very similarly to the positive-parity yrast band in the ''odd-Z core'' ^{81}Y. This is not the case. On the contrary, the crossing frequencies $\hbar\omega\approx 0.57$ MeV (see Fig. 16) of the two signature partners in the middle of Fig. 5 (I) and $\hbar\omega=0.49$ MeV of the band on the right-hand side (II) clearly hint at $g_{9/2}$ proton alignments; i.e., the negative parity is generated by a 2qp neutron excitation. The possible configurations are either $\nu[422]5/2\otimes\nu[303]5/2;\nu[301]1/2$ at moderate prolate deformation or $\nu[321]1/2;\nu[310]1/2 \otimes \nu[422]5/2$ at oblate deformation. The negative-parity band (II) reveals moments of inertia and an alignment pattern very similar to those of the positive-parity yrast cascade in ^{83}Zr (see above). Therefore, this band most probably represents the band built upon an oblate bandhead. Likewise, band (I) might be associated with a near prolate shape, especially since its crossing frequency is about the same as for the $(+,0)$ band in ^{82}Zr.

The generally good agreement between theory and experiment obtained for nuclei with $Z\leqslant 38$ (see discussion above) breaks down for heavier $T_z=1$ nuclei with $Z=39$ (Y) and $Z=40$ (Zr). For both ^{80}Y and ^{82}Zr the theory predicts scenarios with well-deformed ground-state bands being crossed at relatively low frequencies by aligned bands of triaxial shape. However, the relative excitation energy between these prolate and triaxial structures is inconsistent with the data as shown in Fig. 17. It should be pointed out that these inconsistencies arise only when $Z>38$ *and* $N>38$. For example, in the $T_z=3/2$ nuclei $^{77}_{37}\mathrm{Rb}_{40}$ and $^{79}_{38}\mathrm{Sr}_{41}$ the experimental data are reasonably well reproduced by the calculations (see also the discussion for $^{78}_{38}\mathrm{Sr}_{40}$).

Our model suggests that above the $N=Z=38$ deformed shell closure, the vibrational degrees of freedom are becoming more and more important. Figure 18 shows the total Routhian surfaces in $^{82}_{40}\mathrm{Zr}_{42}$ calculated for quasiparticle vacuum at low and high frequencies. Apparently, the low-spin TRS surface is extremely soft in both β_2 and γ directions. For such cases the mean-field model breaks down. The situation changes drastically at higher frequencies: The aligning $g_{9/2}$ quasiparticles drive the nucleus towards a less elongated and triaxial shape. This minimum is well developed; i.e., stiff against vibrations. In fact, this aligned triaxial structure might account for the high-spin portion of the yrast band in $^{82}_{40}\mathrm{Zr}_{42}$ as shown in Fig. 17. Similar conclusions were drawn for the high-spin part of the positive-parity yrast cascade in the next even-even $T_z=1$ nucleus ^{86}Mo from calculations within the configuration-dependent shell-correction approach with a cranked Nilsson potential [74].

IV. CONCLUSIONS

The previously reported high-spin excitation schemes of the weakly populated $T_z=1$ nuclei ^{74}Kr, ^{78}Sr, and ^{82}Zr have been largely extended using the combination of a powerful Ge-detector array (Gammasphere) in conjunction with a selective device such as Microball. The yrast bands are followed up to spins $I\approx 30$ around 20 MeV excitation energy. Altogether 15 new negative- and positive-parity rotational sidebands were identified. In general, the new data confirm the previous high-spin level schemes. The nuclear structure of the two lighter isotopes is dominated by the large shell gaps at large prolate deformation at particle numbers $N,Z=38,40$ while for ^{82}Zr oblate deformed or triaxial minima seem to compete with the well-deformed prolate shape.

We performed systematic calculations for $T_z=1$ nuclei in the mass $A=80$ region using a purely rotational model. The model treats shape and pairing degrees of freedom self-consistently, the former in the sense of the Strutinsky proce-

dure, the latter in terms of the Hartree-Fock-Bogolyubov Lipkin-Nogami theory. Our model does not involve any adjustable parameters. The two-body residual interaction does not involve any neutron-proton interaction. The proton and neutron subsystems are coupled only indirectly by (i) parameters of the mean-field potential and (ii) common deformation. Resonable agreement with the experimental data, concerning excitation energy pattern and alignment, is found in ^{74}Kr, ^{76}Rb, and ^{78}Sr (and in our study in ^{75}Rb and ^{77}Sr, see [58]). The agreement between theory and experiment can be regarded as very good for nuclear many-body theory. We do not find a clear evidence for collective n-p-pairing correlations as one might expect in the vicinity of $N=Z$ line (see also [75,31,33] and references therein). A so-called ''unpaired'' band crossing may have been observed in the positive-parity yrast sequence of ^{78}Sr.

The excited structures find a natural explanation in terms of 2qp configurations (see also [65]). The details concerning the theoretical assignments are discussed in the text. Further evidence was presented for several fp Nilsson orbitals acting as spectators which leads to similar or (in some cases) nearly identical moments of inertia of the respective rotational bands. At low frequencies the shapes corresponding to the configurations discussed here are calculated to be very elongated (see also [2]) with $\beta_2 \approx 0.4$. The associated minima are rather shallow and, therefore, strong shape distortions (shrinking of the quadrupole shape, strong triaxiality effects, and large changes in axial hexadecapole deformation) are predicted to be induced by the aligning $g_{9/2}$ quasiparticles. These predictions can be verified by lifetime measurements.

We associate the disagreement between the theory and experiment found in ^{82}Zr with vibrational degrees of freedom. The total Routhian surfaces calculated for the $Z>38$, $T_z=1$ nuclei reveal pronounced softness at low rotational frequencies with respect to both axial and nonaxial quadrupole degrees of freedom. These vibrational effects are beyond our model and cannot be addressed quantitatively.

ACKNOWLEDGMENTS

The authors would like to thank R. M. Clark, P. Fallon, I. Y. Lee, A. O. Macchiavelli, and R. MacLeod for support during the experiment. D. R. acknowledges the use of the spectrum analysis code VS developed at the University of Cologne and the Radware analysis package. Oak Ridge National Laboratory is managed by Lockheed Martin Energy Research Corp. for the U.S. Department of Energy under Contract No. DE-AC05-96OR22464. This research was supported by an appointment to the Oak Ridge National Laboratory Postdoctoral Research Associates Program administered jointly by the Oak Ridge Institute for Science and Education and Oak Ridge National Laboratory. This work was supported in part by the U.S. Department of Energy under Grant Nos. DE-AC05-76OR00033 (ORISE), DE-FG02-96ER40963 (UT), DE-FG05-87ER40361 (JIHIR), DE-FG05-88ER40406 (WU), and by the National Science Foundation under Grant Nos. PHY-9210082 (FSU) and PHY-9319934 (Pittsburgh). This research was also supported in part by the Polish Committee for Scientific Research under Contract No. 2 P03B 034 08 and the Swedish Natural Science Research Council.

[1] I. Ragnarsson, S. G. Nilsson, and R. K. Sheline, Phys. Rep. **45**, 1 (1978).
[2] W. Nazarewicz *et al.*, Nucl. Phys. **A435**, 397 (1985).
[3] P. Bonche *et al.*, Nucl. Phys. **A443**, 39 (1985).
[4] P.-H. Heenen, P. Bonche, J. Dobaczewski, and H. Flocard, Nucl. Phys. **A561**, 367 (1993).
[5] A. Petrovici, K. W. Schmid, and A. Faessler, Nucl. Phys. **A605**, 290 (1996).
[6] B. J. Varley *et al.*, Phys. Lett. B **194**, 463 (1987).
[7] H. Dejbakhsh *et al.*, Phys. Lett. B **249**, 195 (1990).
[8] M. Wiosna *et al.*, Phys. Lett. B **200**, 255 (1988).
[9] J. Billowes, F. Cristancho, H. Grawe, C. J. Gross, J. Heese, A. W. Mountford, and M. Weiszflog, Phys. Rev. C **47**, R917 (1993).
[10] C. J. Lister, B. J. Varley, H. G. Price, and J. W. Olness, Phys. Rev. Lett. **49**, 308 (1982).
[11] C. Thibault *et al.*, Phys. Rev. C **23**, 2720 (1981).
[12] R. E. Silverans *et al.*, Phys. Rev. Lett. **60**, 2607 (1988).
[13] F. Buchinger *et al.*, Phys. Rev. C **41**, 2883 (1991).
[14] J. Heese *et al.*, Phys. Rev. C **36**, 2409 (1987).
[15] C. J. Gross *et al.*, Nucl. Phys. **A501**, 367 (1989).
[16] L. Lühmann *et al.*, Europhys. Lett. **1**, 623 (1986).
[17] C. Baktash *et al.*, Phys. Lett. B **255**, 174 (1991).
[18] S. L. Tabor *et al.*, Phys. Rev. C **49**, 730 (1994).
[19] D. M. Cullen, Conference on physics From Large γ-ray Detector Arrays, 1994 (LBL-35687, Conf-940888), Vol. I, p. 44.
[20] S. L. Tabor *et al.*, Phys. Rev. C **41**, 2658 (1990).
[21] J. Heese *et al.*, Phys. Rev. C **43**, R921 (1991).
[22] J. Döring (unpublished).
[23] C. Baktash *et al.*, Phys. Rev. Lett. **74**, 1946 (1995).
[24] D. R. LaFosse *et al.*, Phys. Lett. B **354**, 34 (1995).
[25] H.-Q. Jin *et al.*, Phys. Rev. Lett. **75**, 1471 (1995).
[26] A. Harder *et al.*, Phys. Lett. B **374**, 277 (1996).
[27] J. A. Sheikh, N. Rowley, and M. A. Nagarajan, Phys. Lett. B **240**, 11 (1990).
[28] D. Rudolph *et al.*, Phys. Rev. Lett. **76**, 376 (1996).
[29] C. J. Lister *et al.*, Phys. Rev. C **42**, R1191 (1990).
[30] W. Gelletly *et al.*, Phys. Lett. B **253**, 287 (1991).
[31] H. H. Wolter, A. Faessler, and P. U. Sauer, Phys. Lett. **31B**, 516 (1970).
[32] J. Engel, S. Pittel, M. Stoitsov, P. Vogel, and J. Dukelsky, LANL Report nucl-th/9610045, 1996.
[33] W. Satula and R. Wyss, Phys. Lett. B **393** 1 (1997).
[34] C. J. Gross *et al.*, Phys. Rev. C **49**, R580 (1994).
[35] A. Harder *et al.*, Phys. Rev. C **51**, 2932 (1995).
[36] I. Y. Lee, Nucl. Phys. **A520**, 641c (1990).
[37] D. G. Sarantites *et al.*, Nucl. Instrum. Methods Phys. Res. A **381**, 418 (1996).
[38] C. J. Lister *et al.*, Phys. Rev. Lett. **59**, 1270 (1987).
[39] M. K. Kabadiyski, K. P. Lieb, and D. Rudolph, Nucl. Phys. **A563**, 301 (1993).

[40] R. B. Piercey *et al.*, Phys. Rev. Lett. **47**, 1514 (1981).
[41] J. Roth *et al.*, J. Phys. G **10**, L25 (1984).
[42] C. J. Gross *et al.*, Phys. Rev. C **39**, 1780 (1989).
[43] R. F. Davie *et al.*, Nucl. Phys. **A463**, 683 (1987).
[44] C. J. Lister *et al.*, in *Proceedings of the International Symposium on In-Beam Nuclear Spectroscopy, Debrecen*, edited by Z. S. Dombradi and T. Fenyes (Hungarian Academy of Science, Budapest, 1984).
[45] S. Mitarai *et al.*, Z. Phys. A **344**, 405 (1993).
[46] A. A. Chishti *et al.*, Phys. Rev. C **48**, 2607 (1993).
[47] J. Lindhard, V. Nielsen, and M. Scharf, Mat. Fys. Medd. Dan. Vidensk. Selsk. **36**, 10 (1968).
[48] G. Winter, program DESASTOP (unpublished).
[49] G. Winter, Nucl. Instrum. Methods Phys. Res. **214**, 537 (1983).
[50] A. Harder *et al.*, Phys. Rev. C **55**, 1680 (1997).
[51] F. Cristancho *et al.*, Nucl. Phys. **A501**, 118 (1989).
[52] V. M. Strutinsky, Yad. Fiz. **3**, 614 (1966).
[53] S. Cohen, F. Plasil, and W. J. Swiatecki, Ann. Phys. (N.Y.) **82**, 557 (1974).
[54] H. Sakamoto and T. Kishimoto, Nucl. Phys. **A501**, 205 (1989).
[55] H. C. Pradhan, Y. Nogami, and J. Law, Nucl. Phys. **A201**, 357 (1973).
[56] W. Satula, R. Wyss, and P. Magierski, Nucl. Phys. **A578**, 45 (1994).
[57] W. Satula and R. Wyss, Phys. Rev. C **50**, 2888 (1994).
[58] C. J. Gross *et al.* (unpublished).
[59] J. Heese *et al.*, Phys. Rev. C **41**, 1553 (1990).
[60] C. Baktash, J. D. Garrett, D. F. Winchell, and A. Smith, Nucl. Phys. **A557**, 145c (1992).
[61] W. Nazarewicz and T. Werner, in *Nuclear Structure of the Zirconium Region*, edited by J. Eberth, R. A. Meyer, and K. Sistemich (Springer, Berlin, 1988), p. 277.
[62] M. A. Riley, J. D. Garrett, J. Simpson, and J. F. Sharpey-Schafer, Phys. Rev. Lett. **60**, 553 (1988).
[63] J. Döring *et al.*, Phys. Rev. C **52**, R2284 (1995).
[64] S. M. Harris, Phys. Rev. **138**, 509B (1965).
[65] T. Nakatsukasa, K. Matsuyanagi, I. Hamamoto, and W. Nazarewicz, Nucl. Phys. **A573**, 333 (1994).
[66] S. Mitarai *et al.*, Nucl. Phys. **A557**, 381c (1993).
[67] H. Schnare, private communication.
[68] T. D. Johnson *et al.*, Z. Phys. A **350**, 189 (1994).
[69] W. Fieber *et al.*, Z. Phys. A **332**, 363 (1989).
[70] D. Rudolph *et al.*, Z. Phys. A **338**, 139 (1991).
[71] A. W. Mountford *et al.*, Phys. Lett. B **279**, 228 (1992).
[72] J. Dudek, W. Nazarewicz, and N. Rowley, Phys. Rev. C **35**, 1489 (1987).
[73] H. G. Price *et al.*, Phys. Rev. Lett. **51**, 1842 (1983).
[74] D. Rudolph *et al.*, Phys. Rev. C **54**, 117 (1996).
[75] A. Goswami, Nucl. Phys. **60**, 228 (1964).